AD-A145 079 NONLINEAR PROPAGATION IN A DEPTH-DEPENDENT OCEAN(U) 1/1
TEXAS UNIV AT AUSTIN APPLIED RESEARCH LABS C L MORFEY
01 MAY 84 ARL-TR-84-11 N00014-82-K-0805

UNCLASSIFIED F/G 20/1 NL

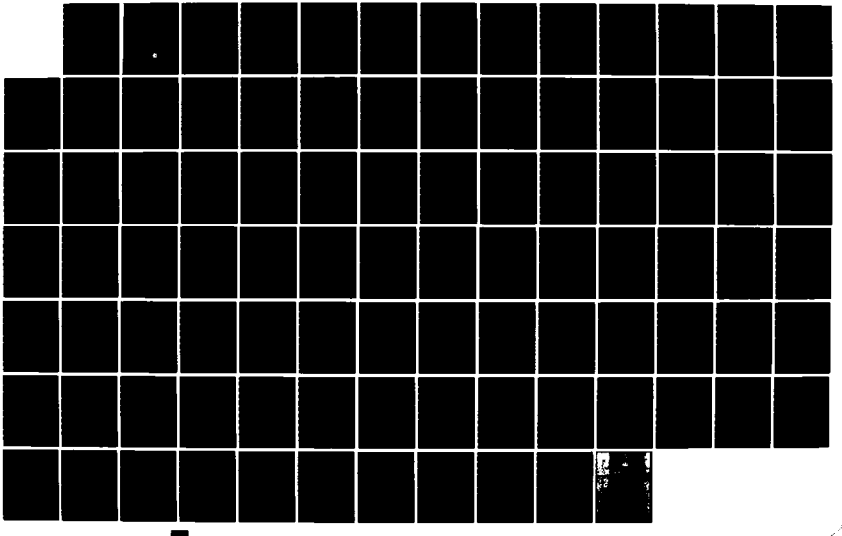

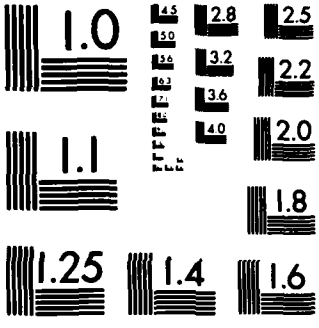

(12)

ARL-TR-84-11

Copy No. 5

NONLINEAR PROPAGATION IN A DEPTH-DEPENDENT OCEAN

Annual Report under Contract N00014-82-K-0805

Christopher L. Morfey

APPLIED RESEARCH LABORATORIES
THE UNIVERSITY OF TEXAS AT AUSTIN
POST OFFICE BOX 8029, AUSTIN, TEXAS 78713-8029

1 May 1984

Annual Report

1 September 1982 - 30 September 1983

Prepared for:

OFFICE OF NAVAL RESEARCH
DEPARTMENT OF THE NAVY
ARLINGTON, VA 22217

UNCLASSIFIED

SECURITY CLASSIFICATION OF THIS PAGE *(When Data Entered)*

REPORT DOCUMENTATION PAGE		READ INSTRUCTIONS BEFORE COMPLETING FORM
1. REPORT NUMBER	2. GOVT ACCESSION NO. AD-A145079	3. RECIPIENT'S CATALOG NUMBER
4. TITLE *(and Subtitle)* NONLINEAR PROPAGATION IN A DEPTH-DEPENDENT OCEAN		5. TYPE OF REPORT & PERIOD COVERED Annual Report / 1 Sep 82 - 30 Sep 83
		6. PERFORMING ORG. REPORT NUMBER ARL-TR-84-11
7. AUTHOR(s) C. L. Morfey		8. CONTRACT OR GRANT NUMBER(s) N00014-82-K-0805
9. PERFORMING ORGANIZATION NAME AND ADDRESS Office of Naval Research Department of the Navy Arlington, VA 22217		10. PROGRAM ELEMENT, PROJECT, TASK AREA & WORK UNIT NUMBERS
11. CONTROLLING OFFICE NAME AND ADDRESS		12. REPORT DATE 1 May 1984
		13. NUMBER OF PAGES 94
14. MONITORING AGENCY NAME & ADDRESS *(if different from Controlling Office)*		15. SECURITY CLASS. *(of this report)* UNCLASSIFIED
		15a. DECLASSIFICATION/DOWNGRADING SCHEDULE

16. DISTRIBUTION STATEMENT *(of this Report)*

Approved for public release; distribution unlimited.

17. DISTRIBUTION STATEMENT *(of the abstract entered in Block 20, if different from Report)*

18. SUPPLEMENTARY NOTES

19. KEY WORDS *(Continue on reverse side if necessary and identify by block number)*

nonlinear propagation
finite amplitude effects
ray theory
long range propagation
ocean acoustics
underwater explosions
stratified ocean

20. ABSTRACT *(Continue on reverse side if necessary and identify by block number)*

The propagation of finite-amplitude sound in a depth-dependent ocean has been studied analytically and numerically, using a model based on weak-shock theory and the high frequency ray approximation. Results are presented for the equivalent propagation distance, in a uniform ocean, which reproduces the nonlinear distortion in the real situation. Numerical results for typical

DD FORM 1 JAN 73 1473 EDITION OF 1 NOV 65 IS OBSOLETE

UNCLASSIFIED

SECURITY CLASSIFICATION OF THIS PAGE *(When Data Entered)*

20. (cont'd)

ocean profiles are collapsed by means of an asymptotic theory, for ray paths along which the sound speed increases or decreases monotonically. Results are also shown for rays which form caustics.

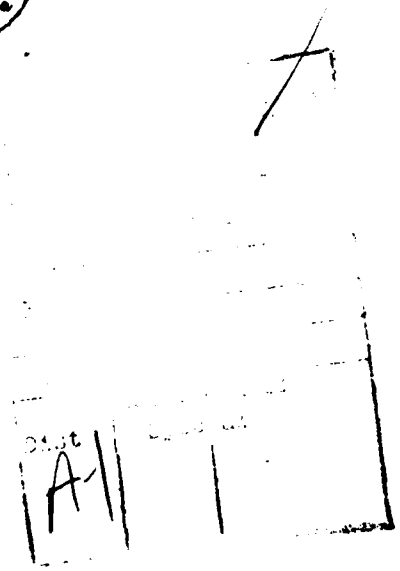

TABLE OF CONTENTS

LIST OF FIGURES

LIST OF TABLES

PREFACE

This is the first annual report on Contract N00014-82-K-0805, "Nonlinear Effects in Long Range Propagation." The study has been organized under three task headings as follows

Task I--Shock pulse propagation in a homogeneous ocean
Task II--Nonlinear propagation in a depth-dependent ocean
Task III--Nonlinear propagation in a caustic region

Considerable progress has been made in all three tasks. In the present report, however, attention is focused on Task II. The investigation of inhomogeneous ocean effects presented in this report is complete, and Task II is accordingly regarded as accomplished.

A further report is in preparation which will summarize the substantial progress made to date on Task III. Also prior to the final report a paper is to be prepared on the Task I study, for presentation at the 10th International Symposium on Nonlinear Acoustics, Kobe, Japan (25-28 July 1984).

I. INTRODUCTION

In a real ocean whose properties are not uniform, but vary slowly--on a wavelength scale--with position, the propagation of finite-amplitude acoustic signals differs in three important ways from that in a uniform medium.

(a) Ray paths are curved (Fig. 1, page 5), and ray tube areas are no longer proportional to s^2. The inverse-distance spreading law for weak waves is replaced by

$$(S/\rho c)^{1/2}\, p(t',s) = f(t') \quad \text{(lossless medium)}, \tag{1}$$

where S is the ray tube area, and

$$t' = t - \int ds/c \tag{2}$$

defines the retarded time for outgoing waves of small amplitude.

(b) Cumulative nonlinear distortion of the signal is described (as in the case of a homogeneous medium) by replacing the linear retarded time variable in Eq. (1) with a modified time variable τ. However, the nonlinear part of τ grows at a variable rate along the ray path, which depends not only on S(s) but also on the local fluid properties $\beta(s)$, $\rho(s)$, c(s).

(c) The rates of attenuation and dispersion in a real (lossy) medium are additionally dependent on position.

As a first step towards a model which includes all of these effects, we consider the following approximation. Finite-amplitude sound in a lossless ocean is considered as propagating along the ray paths followed by small-signal waves. Self-refraction of the signal wavefronts is thus neglected. Furthermore, the only losses in our model are those which occur at shocks in the waveform.

Within this context, we are able to introduce a generalized version of the reduced propagation distance ($\bar{x}$) to account for effects (a) and (b) above. Analytical

results have been obtained for the reduced distance by assuming a horizontally stratified ocean with simplified property profiles. To allow for realistic variations of temperature, pressure, and salinity with depth, a program has been written to evaluate $\bar{x}$ numerically, and results for some typical profiles are presented.

Finally, we note that the importance of the $\bar{x}$ generalization lies in the fact that all the predictions of weak-shock theory for a uniform ocean become available for the nonuniform case, merely through substitution of the appropriate $\bar{x}$ value.

II. LITERATURE SURVEY

The generalization of ray theory to allow for nonlinear waveform steepening in a slowly varying medium has been discussed in detail by Carlton and Blackstock[1] and Pelinovskii, Petukhov and Fridman.[2] Their results are stated in terms of a reduced propagation distance, denoted here by $\bar{x}$. Physically, $\bar{x}$ represents the plane wave propagation distance, in a medium of properties (ρ_o, c_o), which yields the same amount of nonlinear distortion as propagation along the actual ray path from s_o to s. Mathematically, $\bar{x}$ is given by an integral expression along the ray path; a simplified derivation is given at the beginning of Section III.

Following an inconclusive earlier paper by Fridman,[3] Petukhov and Fridman[4] addressed the overall problem of describing blast-wave parameters in a stratified ocean. They used the weak-shock model to obtain the departures, from their homogeneous ocean values, of the peak pressure (p_s), time constant (θ_s), and related signal properties. It is important to recognize that much of the deviation which they report from the reference case is a consequence purely of linear acoustics (i.e., ray curvature).

To explain this last point, we note that linear ray acoustics predicts different values of $p_s(s)$--at the same distance s--along different rays in an inhomogeneous ocean. The variation arises from the factor $(S/\rho c)^{1/2}$ in Eq. (1), and has nothing to do with the nonlinear effects which are the subject of the present report.

In the present study we avoid confusion between the linear and nonlinear effects of ocean property variations, by focusing specifically on the reduced distance. A knowledge of $\bar{x}$ completely characterizes the nonlinear properties of a given propagation path, within the framework of weak-shock theory. Consequently it appears preferable to present information on $\bar{x}$ for different ocean profiles, ray launch angles, etc., and leave the user to draw conclusions appropriate to whatever particular initial waveform is of interest.

The calculation of $\bar{x}$ in any particular case requires a knowledge of the nonlinearity coefficient (β), density (ρ), and sound speed (c) as a function of position. In seawater these properties are related to the local temperature (T), salinity (S), and pressure (P). Convenient approximations are given in Refs. 5 through 9, and cover conditions encountered in most of the earth's oceans.[10] The relevant formulae needed for the present study have been assembled in Appendix B.

III. ANALYSIS OF NONLINEAR PROPAGATION IN A SLOWLY VARYING OCEAN

A. Definition of Reduced Distance

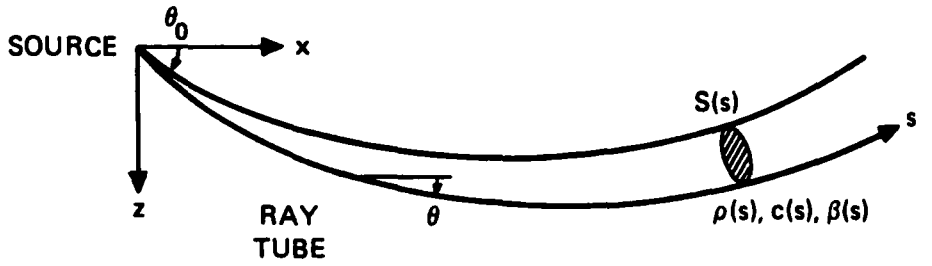

FIGURE 1

DEFINITION SKETCH FOR RAY TUBE IN DEPTH-DEPENDENT OCEAN

The propagation distance s is measured from the source, along the curved ray path.

As indicated in the Introduction, we expect the quantity $Sp^2/\rho c$ (where p is the acoustic pressure) to remain constant following a progressive wavelet. The wavelet propagation speed, along the ray tube in Fig. 1, is modified at finite amplitudes to

$$c(s) + \beta(s)u \simeq c + \frac{\beta}{\rho c}\, p \ . \tag{3}$$

Here β is the nonlinearity parameter, and u is the particle velocity.

A solution for progressive waves, to first order accuracy in p, is therefore of the form

$$\left(\frac{S}{\rho c}\right)^{1/2} p = f\left\{t - \int \frac{ds}{c + (\beta/\rho c)p}\right\}$$

$$\simeq f(t' + \int \frac{\beta}{\rho c^3}\, p\, ds) \ , \tag{4}$$

where the retarded time t' is defined by Eq. (2). Equation (4) may be reduced to the standard form for nonlinear plane waves in a homogeneous medium, by means of the substitutions

$$\bar{p} = p\left(\frac{S}{S_o}\right)^{1/2}\left(\frac{\rho c}{\rho_o c_o}\right)^{-1/2} \quad \text{(reduced pressure)} \tag{5}$$

and

$$\bar{x} = \int_{s_o}^{s} \frac{\alpha}{\alpha_o}\left(\frac{S}{S_o}\right)^{-1/2} ds' \quad \text{(reduced distance)} \ . \tag{6}$$

Here α is a thermodynamic property of the medium, defined by

$$\alpha = \beta(\rho c^5)^{-1/2} \ . \tag{7}$$

The reference ray tube area S_o refers to a position close enough to the source that the rays are still straight; it will be replaced later in terms of an arc length (or initial distance) s_o.

The solution in terms of reduced variables $\bar{p}$, $\bar{x}$ is thus

$$\bar{p} = f\left(t' + \frac{\beta_o}{\rho_o c_o^3}\,\bar{x}\,\bar{p}\right) , \tag{8}$$

in which the subscript o denotes reference values, chosen for convenience to match the properties of the source region. The reduced quantities $\bar{p}$, $\bar{x}$ may be interpreted as the plane wave pressure and propagation distance in the reference medium.

It is convenient for later purposes to express the reduced distance $\bar{x}$ as

$$\bar{x} = s_o \ln\left(\frac{s}{s_o} G\right) \ ; \tag{9}$$

numerical results for the dimensionless factor G are presented in the remainder of this report. Note that the function G is equal to 1 for a homogeneous ocean, in which case s is simply the radial range and Eq. (9) reduces to the usual expression for simple radial waves.

Departures of G from 1 indicate modification of the effective propagation distance by the combined effects of ray tube geometry and medium inhomogeneity. In particular $G > 1$ implies that distortion develops more rapidly than for spherical waves in a homogeneous medium, and $G < 1$ that distortion develops more slowly.

B. Analytical Formulation of $\bar{x}$ Integral in Terms of Ray Coordinates

The ray tube area ratio in Eq. (6) may be expressed as

$$\frac{S}{S_o} = \frac{x\xi}{x_o^2} \sin\theta \cos\theta_o \quad , \quad \left[\xi = \left(\frac{\partial x}{\partial \theta_o}\right)_z\right] \tag{10}$$

or equivalently as

$$\frac{S}{S_o} = \frac{x\zeta}{x_o^2} \cos\theta \cos\theta_o \quad , \quad \left[\zeta = \left(\frac{\partial z}{\partial \theta_o}\right)_x\right] \quad . \tag{11}$$

Here θ (see Fig. 1) is the ray angle, and θ_o is the ray launch angle; x is the horizontal range, and x_o (corresponding to S_o) is the reference value near the source. These expressions assume a horizontally stratified ocean and axisymmetric (cylindrical) spreading. Equation (10) is the form used by Petukhov and Fridman;[4] Eq. (11) is the form used at ARL:UT in the MEDUSA ray tracing program.[11]

For any given sound speed profile, the ray coordinates (x,z) and the launch angle derivatives (ξ or ζ) may be calculated. Then if the α profile is also specified, Eq. (6) for $\bar{x}$ may be evaluated by integration.

In general the result will not be expressible analytically in closed form. However, some useful analytic results have been obtained by assuming a power law relation between α and c, of the form

$$\frac{\alpha}{\alpha_o} = \left(\frac{c}{c_o}\right)^{-n} \quad . \tag{12}$$

These are described below. For a discussion of the validity of Eq. (12), see Appendix C.

C. Explicit Analytic Results for a Linear Sound Speed Profile

By using the known solution for ray trajectories in this case, we find

$$\frac{S}{S_o} = \left(\frac{s}{s_o}\right)^2 \sec^2\theta_o \left(\frac{\sin\theta - \sin\theta_o}{\theta - \theta_o}\right)^2 \quad . \tag{13}$$

Note that $s/(\theta - \theta_o)$ is a constant along each ray, equal to the radius of curvature. Substituting in Eq. (6), and using Eq. (12) along with

$$\frac{c}{c_o} = \frac{\cos\theta}{\cos\theta_o} \quad , \tag{14}$$

gives in the limit of small s_o

$$\bar{x} = \lim_{s_o \to 0} \; s_o \cos\theta_o \cdot \int_{\theta(s_o)}^{\theta} \frac{d\theta}{(\sin\theta - \sin\theta_o)} \left(\frac{\cos\theta_o}{\cos\theta}\right)^n \quad . \tag{15}$$

Since the integral in Eq. (15) can be expressed in closed form for $n=\pm 1$ and $n=0$, the function G can be found for these cases. In particular, the case $n=1$ gives [using formula 2.561(5) in Gradshteyn and Ryzhik's Table of Integrals[12]]

$$G(\theta_o,\theta) = \frac{\sin\theta - \sin\theta_o}{(\theta - \theta_o)\cos\theta} \cdot \left\{\frac{\tan(\frac{\pi}{4} + \frac{\theta}{2})}{\tan(\frac{\pi}{4} + \frac{\theta_o}{2})}\right\}^{\sin\theta_o} \quad . \tag{16}$$

This result is of interest since equation (12) with $n=1$ gives a reasonable approximation to the deep ocean behavior of α (see Appendix C).

The case n=0 corresponds to the assumption of constant α in the reduced distance integral, Eq. (6). Although not claimed to be realistic, it provides a useful comparison. The resulting expression for G [obtained using formula 2.551(3) in the Table of Integrals[12]] is

$$G(\theta_o, \theta) = \frac{\tan\frac{1}{2}\theta - \tan\frac{1}{2}\theta_o}{(\theta - \theta_o)} \quad \frac{4\cos\theta_o \cos^2\frac{1}{2}\theta_o}{1 + \cos\theta_o - \sin\theta_o \tan\frac{1}{2}\theta} \quad . \tag{17}$$

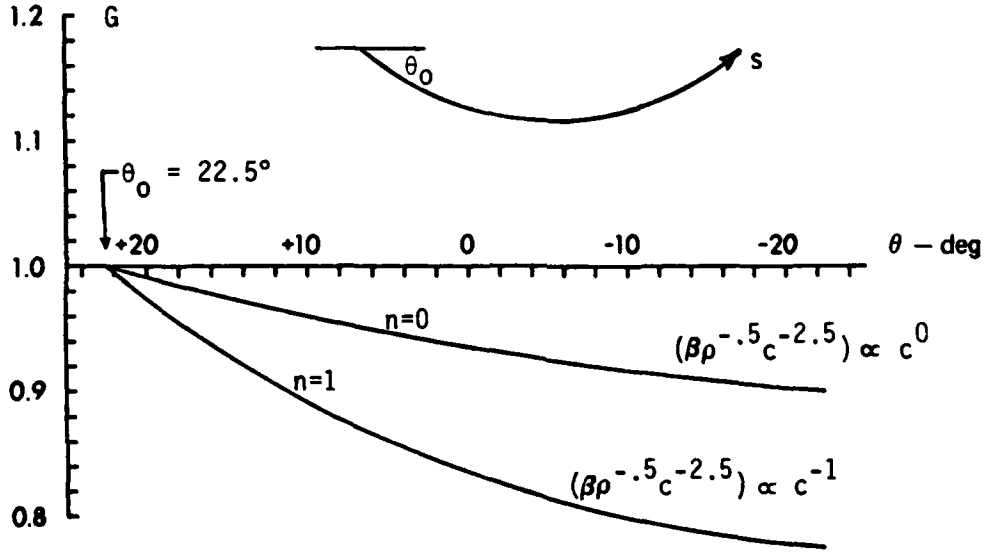

FIGURE 2

DISTANCE MODIFICATION FACTOR G PLOTTED AGAINST RAY ANGLE

Results based on analytic solution for a linear sound speed profile.

Figure 2 shows G(n=1) and G(n=0) plotted against θ, for an initial launch angle of 22.5° (in the direction of increasing c). A significant conclusion may immediately be drawn: variation of ocean properties with depth has an important direct effect on the reduced distance (through the α factor in Eq. (6)), which is comparable with the effect of nonspherical spreading.

D. Asymptotic Approximations for Nonlinear Sound Speed Profiles

Analytic results for G may also be obtained for more general profiles by treating the relative variation in sound speed as a small quantity. Thus we assume the quantity

$$\sigma = \left(\frac{c}{c_o} - 1\right) \tag{18}$$

to have a numerical value much less than 1.

It is convenient to define the sound speed profile in inverse form, by expressing z as a second-degree polynomial in σ:

$$\frac{z}{a} = \sigma - \frac{1}{2} b\sigma^2 \quad \text{(a,b constants)} \ . \tag{19}$$

This allows a first-order (in σ) departure from linearity.

If the $\bar{x}$ integral is evaluated using Eq. (19), and is consistently approximated to first-order accuracy in σ, we obtain the following expression for the factor G as defined in Eq. (9):

$$G \simeq 1 - (n + \tfrac{1}{2})\sigma \quad . \tag{20}$$

Details of the analysis are given in Appendix D. On the other hand, expanding the available exact solutions for n=1 (Eq. 16) and n=0 (Eq. (17) in powers of $(\theta - \theta_o)$ yields the first-order approximations

$$G(n = 1) \simeq \left(\frac{c}{c_o}\right)^{-3/2} \simeq 1 - \frac{3}{2}\sigma \quad , \tag{21}$$

$$G(n = 0) \simeq \left(\frac{c}{c_o}\right)^{-1/2} \simeq 1 - \frac{1}{2}\sigma \quad . \tag{22}$$

These evidently agree with Eq. (20) as special cases. Since neither the profile curvature parameter b, nor the launch angle θ_o, appears in the above results, a useful conclusion emerges from the asymptotic analytical treatment--namely that the distance modification factor G is principally a function of the sound speed ratio c/c_o, and only secondarily a function of ray launch angle and the precise shape of the c(z) profile. The predicted trend of G with c/c_o is given by Eq. (20) as

$$G \propto \left(\frac{c}{c_o}\right)^{-(n + 1/2)} , \tag{23}$$

where n is the index in the approximate α versus c relation, Eq. (12).

However, a condition attached to all these asymptotic results is that the ray angle must not approach zero (horizontal propagation), since the series expansions in Appendix D break down at this point. As a consequence, Eq. (23) cannot be applied to a ray which has passed through a vertex.

In the remainder of this report, we present exact analytic and also numerical calculations of G for particular cases. By plotting G as a function of c/c_o for different launch angles and ocean profiles, we are able to test the conclusions reached above.

E. Comparison of Exact and Asymptotic Predictions for the Linear Profile Case

We begin by testing Eq. (23) against a case for which Eq. (16) provides an exact analytic solution: namely the idealized linear sound speed profile with αc constant. Values of the distance modification factor G, calculated from Eq. (16), are plotted in Fig. 3 against c/c_o. Both downward-propagating rays (launch angles θ_o=15°, 22.5°, 30°, 45°, 60°, 75°) and upward-propagating rays (θ_o=0°, -15°, -30°, -45°, -60°, -75°) are shown.

The breakdown of the asymptotic $(c/c_o)^{-3/2}$ prediction, given by Eq. (23) with n=1, is apparent for near-horizontal rays as expected. Figure 3 shows that the asymptotic prediction is nevertheless quite accurate for launch angles more than 30°

from the horizontal in either direction. The curves for $\theta_o = \pm 60°$ and $\pm 75°$ are barely distinguishable from the asymptote.

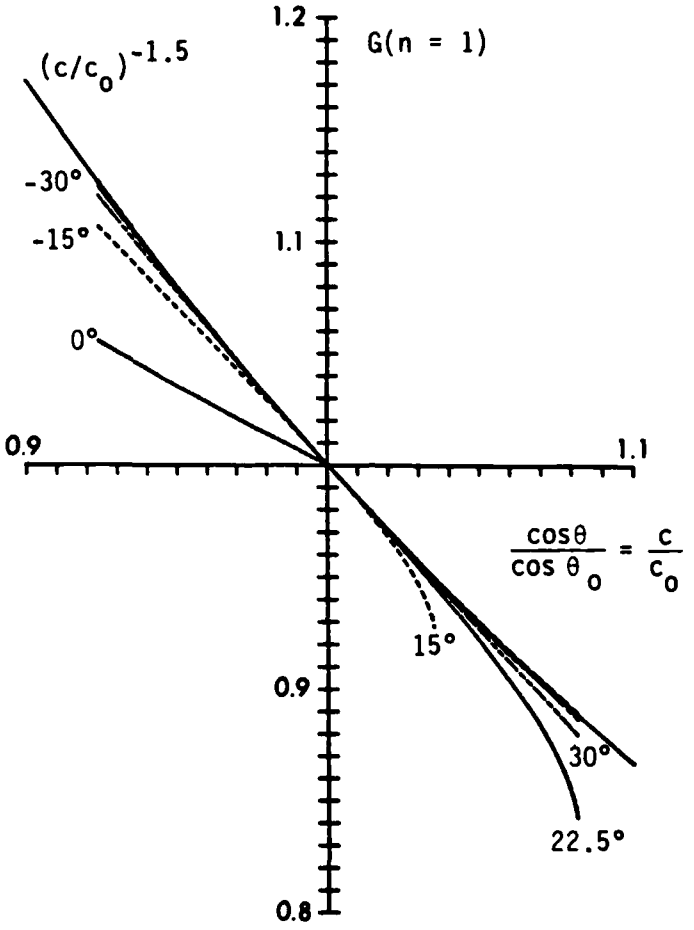

FIGURE 3

PLOT OF G VERSUS SOUND SPEED RATIO

This plot, for a linear sound speed profile, shows results assuming c constant. The asymptotic $(c/c_o)^{-3/2}$ prediction is shown, together with the exact analytic calculation for selected launch angles (as marked on each curve). The rays launched at 15° and 22.5° have been terminated at their vertex points.

In Section IV below, we describe a numerical scheme for evaluating the factor G along any ray path, and results are presented for more realistic ocean profiles. These provide a more searching test of the asymptotic theory, and also allow a study of caustic formation.

IV. COMPARISON OF NUMERICAL AND ASYMPTOTIC PREDICTIONS FOR TYPICAL OCEAN PROFILES

Since analytic expressions for G, such as Eqs. (16) and (17), are available only for highly idealized profiles of c(z) and $\alpha(z)$, a parallel objective has been the development of an efficient numerical code with which G can be evaluated numerically, for any variation of ocean properties with depth.

The objective has been met by adding on to the ARL:UT MEDUSA program a post-processing stage, which takes MEDUSA output quantities (such as ray angle, path length, etc.) and performs a numerical integration along the ray path to arrive at G. The method is described in detail in Appendix F. MEDUSA is a versatile and accurate ray tracing program developed at ARL:UT by T. L. Foreman and described in Ref. 11.

A. Accuracy of Numerical Solution

The numerical calculation scheme has been tested against the known exact solution for G, Eq. (16), for a linear c(z) profile with αc=constant. The test case was specified by

$$c = c_o(1 + z/a) \quad , \quad a = 88{,}800 \text{ m}; \tag{24}$$

downward-going rays were launched at angles θ_o=15°, 22.5°, and 60° from depth z=0, and allowed to propagate to z = 2900 m. Table I compares the numerical results for horizontal range, x, and the nonlinear distance modification factor, G, with the exact analytical predictions (x_a, G_a) for each case. The quantities tabulated are $x-x_a$, in meters, and the relative error $|G-G_a|/|G_a-1|$. Note that the first of these indicates the accuracy of the basic ray tracing program, while the second is a measure of the combined program accuracy.

The first row in Table I gives the errors for the most accurate version of the numerical calculation. Here the profiles c(z) and $\alpha(z)$ are specified analytically. By the end of the propagation path, the accumulated relative error in G is only of order 10^{-5}. This is a measure of the accuracy of the ray path solver, which is further

TABLE I. ERRORS IN COMPUTED NONLINEAR RANGE FACTOR G, AND HORIZONTAL RANGE x

Propagation through a constant-gradient layer at different launch angles (in direction of increasing c). Layer thickness = 2900 m; sound speed ratio 1.033 (a = 88 800 m). The numbers N_c, N_α denote the number of points used to define the sound speed and α profiles (see text). Results computed on the ARL:UT CYBER machine with 32-bit word length.

		$\theta_o = 15°$		$\theta_o = 22.5°$		$\theta_o = 60°$	
N_c	N_α	$x-x_a$ (m)	$\left\|\frac{G-G_a}{1-G_a}\right\|$	$x-x_a$ (m)	$\left\|\frac{G-G_a}{1-G_a}\right\|$	$x-x_a$ (m)	$\left\|\frac{G-G_a}{1-G_a}\right\|$
∞	∞	-0.106	$1.0\ 10^{-5}$	-0.010	$1.0\ 10^{-5}$	0.001	$1.7\ 10^{-5}$
∞	10	-0.106	$2.8\ 10^{-4}$	-0.010	$3.3\ 10^{-4}$	-0.001	$2.7\ 10^{-4}$
25	25	-0.139	$9.7\ 10^{-3}$	-0.014	$7.0\ 10^{-3}$	0.000	$2.0\ 10^{-3}$
10	10	-1.55	$2.8\ 10^{-2}$	-0.15	$1.0\ 10^{-2}$	0.005	$7.4\ 10^{-4}$

indicated by the small errors in horizontal range (a few millimeters, except for the shallowest ray).

Subsequent rows in Table I show a progressive loss in accuracy as fewer points are used to specify the c(z) and α(z) profiles. Interpolation of c and α values is achieved by joining the profile points with straight lines in the (1/c, z) plane and the (α, z) plane respectively. The resulting corners are rounded locally by cubic splines, in order to make the profiles continuous through the first two derivatives (i.e., no jumps in profile slope or curvature). As a result of the interpolation scheme, even though the c(z) input points lie on a straight line, they are not interpolated by a straight line in the program; and the smaller the number (N_c) of profile points, the more the interpolated profile deviates from the ideal straight line case.

Table I shows that reducing the number of points in the sound speed profile increases the errors in x and G (with the exception of the 60° ray path example, where the 10-point G calculation is unexpectedly accurate). Note that the increasing errors which appear as the number N_c is reduced are not controlled by the finite step size in the ray tracing program. In fact the step size varies according to the local curvature along the ray path, being automatically selected to meet an accuracy criterion. As a result the analytic c(z) calculation requires fewer steps--by a factor of about 4--than either of the calculations for finite N_c.

We conclude from Table I that a relative error in (G-1) of less than 3 percent is provided by the present numerical scheme, for ocean profiles which are specified by at least 10 points (and preferably by 25 or more). The critical number is N_c (the number of points defining the sound speed profile), since this affects the accuracy of the resulting ray path.

The 3 percent figure in fact represents a considerable achievement, since $|G_a-1|$ is a small number (varying in the example from zero at the beginning of the propagation path to 0.045 at the end; cf. Eq. (21)). It is interesting to note that this accuracy is degraded if care is not taken in transferring MEDUSA output data to the integration program; in order to avoid rounding errors, the data was transferred in octal representation, with full accuracy retained.

B. Specification of Ocean Profiles for Numerical Calculations

In order to arrive at $c(z)$ and $\alpha(z)$ profiles which are consistent with real ocean properties, it is convenient to begin with temperature and salinity profiles $T(z)$ and $S(z)$. The hydrostatic pressure $P(z)$ is conveniently given by Leroy's formula, Ref. 5. Appendix B summarizes the relations between these quantities.

Since nonlinear effects are most likely to occur over propagation paths of several kilometers, we are principally concerned with ocean properties in the deep sound channel and down to depths of around 10 km. Conditions within the first 200 m below the surface, which are much more variable, are not important for the present study.

Some typical deep ocean temperature and salinity profiles, taken from Refs. 13 and 14, are shown in Figs. 4 and 5, respectively. The general pattern is a rapid drop in temperature with increasing depth between about 200 m and 1000-2000 m, followed by a leveling off. Thus the temperature is almost constant at greater depths. The salinity profiles in the North Atlantic show a trend similar to the temperature, but there is relatively little salinity variation over the whole water column in the North Pacific profiles.

Based on these trends, "representative" idealized profiles have been constructed for both $T(z)$ and $S(z)$, made up of 2 or 3 straight-line segments. The profile points are specified in Table II; they are also marked on Figs. 4 and 5. One pair of profiles (open circles) represents the North Atlantic, around a latitude of 20° N. The other pair (solid circles) represents the North Pacific, around 36° N.

C. Sound Speed Profiles and Computed Ray Paths

The sound speed at 35 specified depths, distributed over the water column between the surface and a depth of 10 km, was computed from the temperature and salinity data in Table II. The results are listed in Table III, and the profiles are plotted in Fig. 6. With the tabulated $c(z)$ data as input, ray paths were then calculated using the MEDUSA ray tracing program. This was done for each of the

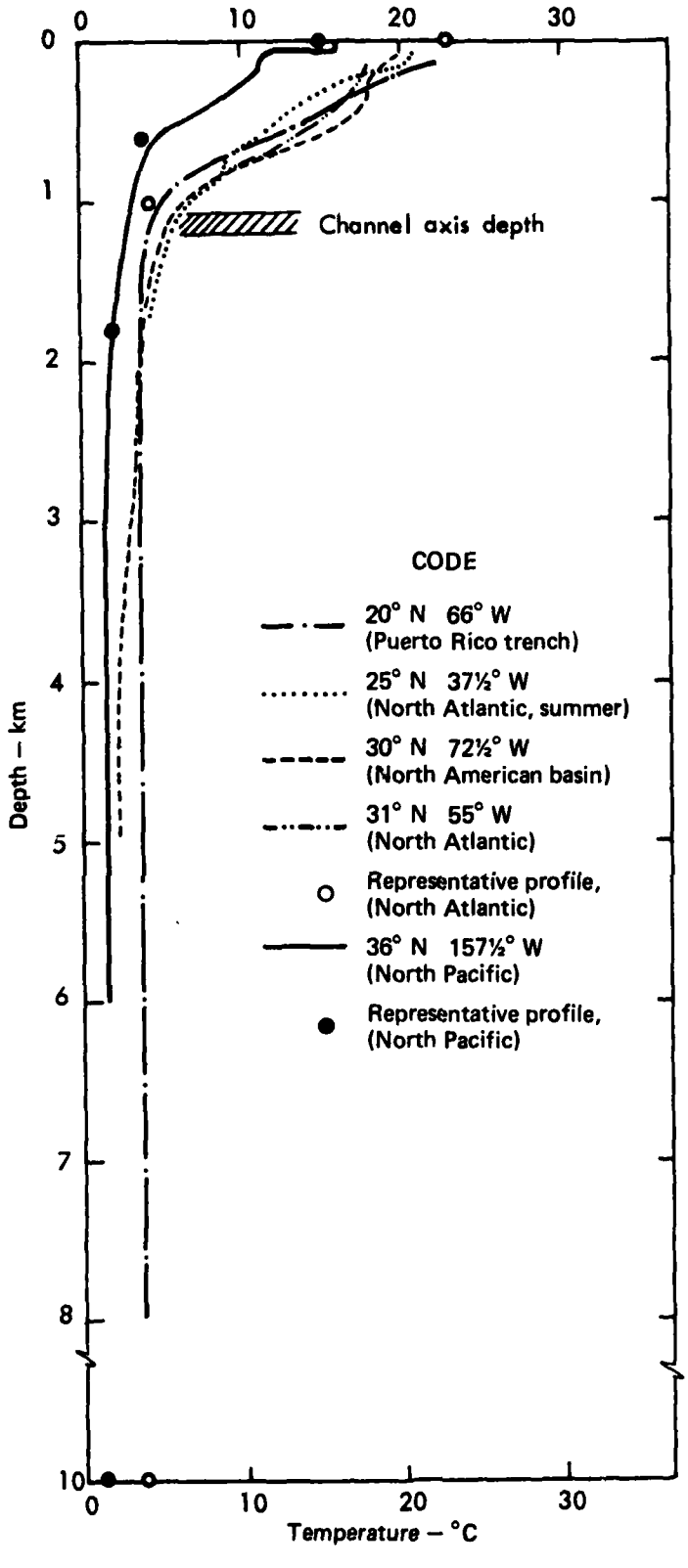

FIGURE 4
TEMPERATURE PROFILES MEASURED IN DEEP OCEAN REGIONS

ARL:UT
AS-84-495
DTB - GA
6 - 11 - 84

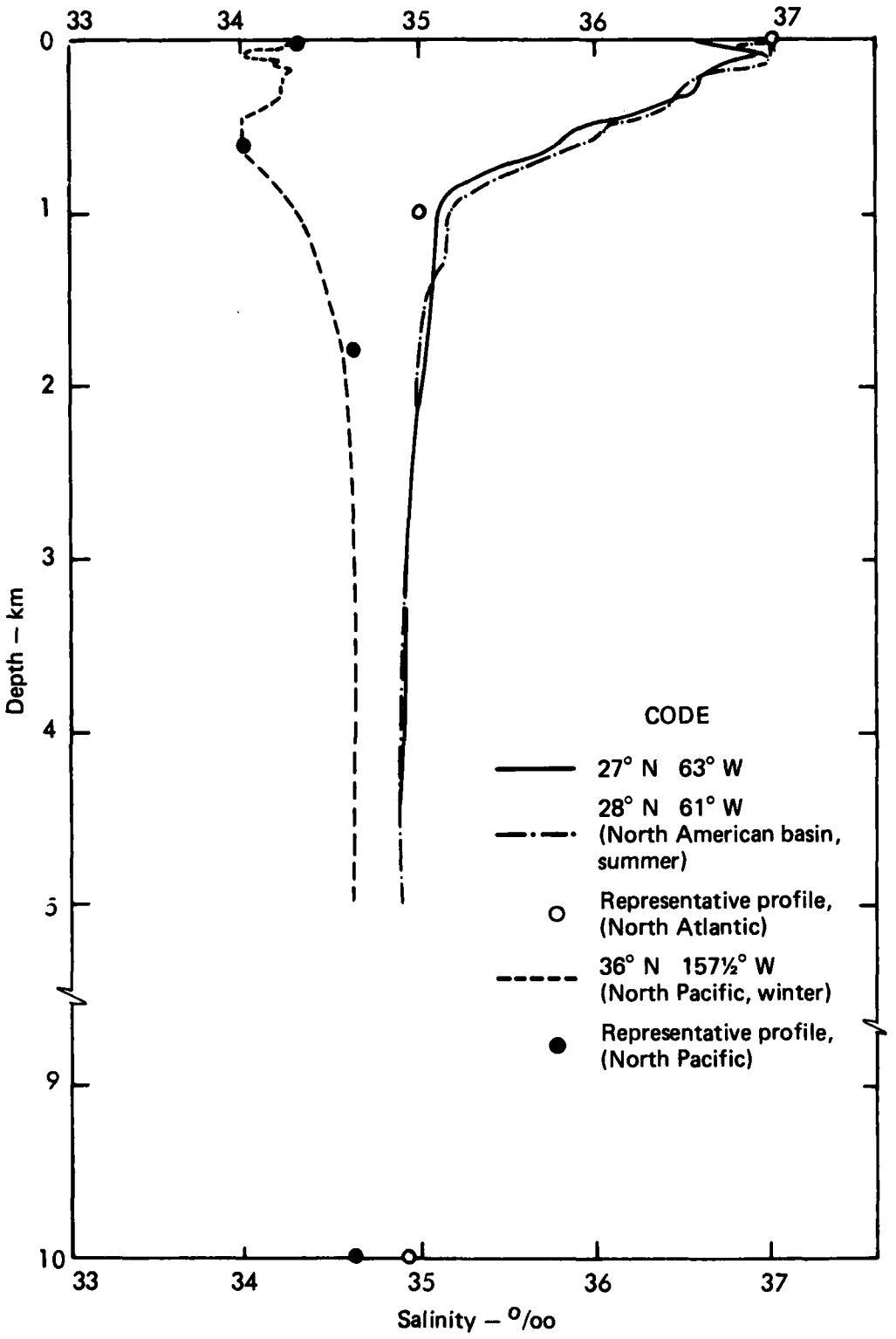

FIGURE 5
SALINITY PROFILES MEASURED IN DEEP OCEAN REGIONS

ARL:UT
AS-84-496
DTB - GA
6 - 11 - 84

TABLE II. IDEALIZED TEMPERATURE AND SALINITY PROFILES USED FOR NUMERICAL CALCULATIONS

Location	Depth,z (m)	Temperature,T (°C)	Salinity,S (°/oo)
N. Atlantic	0	23	37.0
(20° N)	1,000	4.5	35.0
	10,000	3.5	34.9
N. Pacific	0	15	34.3
(36° N)	600	4	34.0
	1,800	2	34.6
	10,000	1	34.6

standardized ocean profiles, using 3 different source depths; from each source depth, 5 or 6 rays were launched at different angles. The results are summarized in Figs. 7, 8, and 9.

Figure 7 shows the resulting ray paths for the North Atlantic profile. For source depths (z_o) of 200 m and 1200 m, the shallower rays exhibit a vertex: we note that the asymptotic analysis of Section III gives no guidance beyond this point. Furthermore, the rays in Fig. 7(b) launched from near the sound channel axis (z_o = 1200 m) at angles of 0° and 7.5° are confined to the sound channel.

The channeled rays exhibit caustic formation (at approximately 8 km and 29 km horizontal range respectively), at which point the concept of a distance modification factor based on nonlinear ray acoustics breaks down. Accordingly, in the results which follow the calculation of G may be terminated for one of three reasons:

(a) The ray reaches the ocean surface.

TABLE III. SOUND SPEED PROFILES DERIVED FROM THE IDEALIZED TEMPERATURE AND SALINITY PROFILES OF TABLE II

(a) North Atlantic			(b) North Pacific		
#	Depth (m)	Speed (m/sec)	#	Depth (m)	Speed (m/sec)
1	0	1532.260	1	0	1506.533
2	10	1531.942	2	10	1506.106
3	20	1531.622	3	20	1505.677
4	30	1531.299	4	30	1505.244
5	40	1530.973	5	40	1504.809
6	50	1530.644	6	50	1504.370
7	70	1529.979	7	70	1503.483
8	90	1529.302	8	90	1502.584
9	110	1528.614	9	110	1501.672
10	150	1527.203	10	150	1499.811
11	200	1525.375	11	200	1497.413
12	250	1523.472	12	250	1494.937
13	300	1521.494	13	300	1492.382
14	400	1517.307	14	400	1487.035
15	500	1512.807	15	500	1481.373
16	600	1507.986	16	600	1475.460
17	700	1502.842	17	700	1476.423
18	800	1497.374	18	800	1477.447
19	1000	1485.535	19	1000	1479.499
20	1200	1488.710	20	1200	1481.557
21	1600	1495.229	21	1600	1485.690
22	2200	1505.096	22	2200	1494.368
23	2800	1515.071	23	2800	1504.368
24	3400	1525.155	24	3400	1514.486
25	4000	1535.348	25	4000	1524.721
26	4600	1545.645	26	4600	1535.073
27	5200	1556.045	27	5200	1545.539
28	5800	1566.542	28	5800	1556.114
29	6400	1577.130	29	6400	1566.794
30	7000	1587.802	30	7000	1577.572
31	7600	1598.550	31	7600	1588.440
32	8200	1609.362	32	8200	1599.390
33	8800	1620.228	33	8800	1610.410
34	9400	1631.133	34	9400	1621.488
35	10000	1642.065	35	10000	1632.611

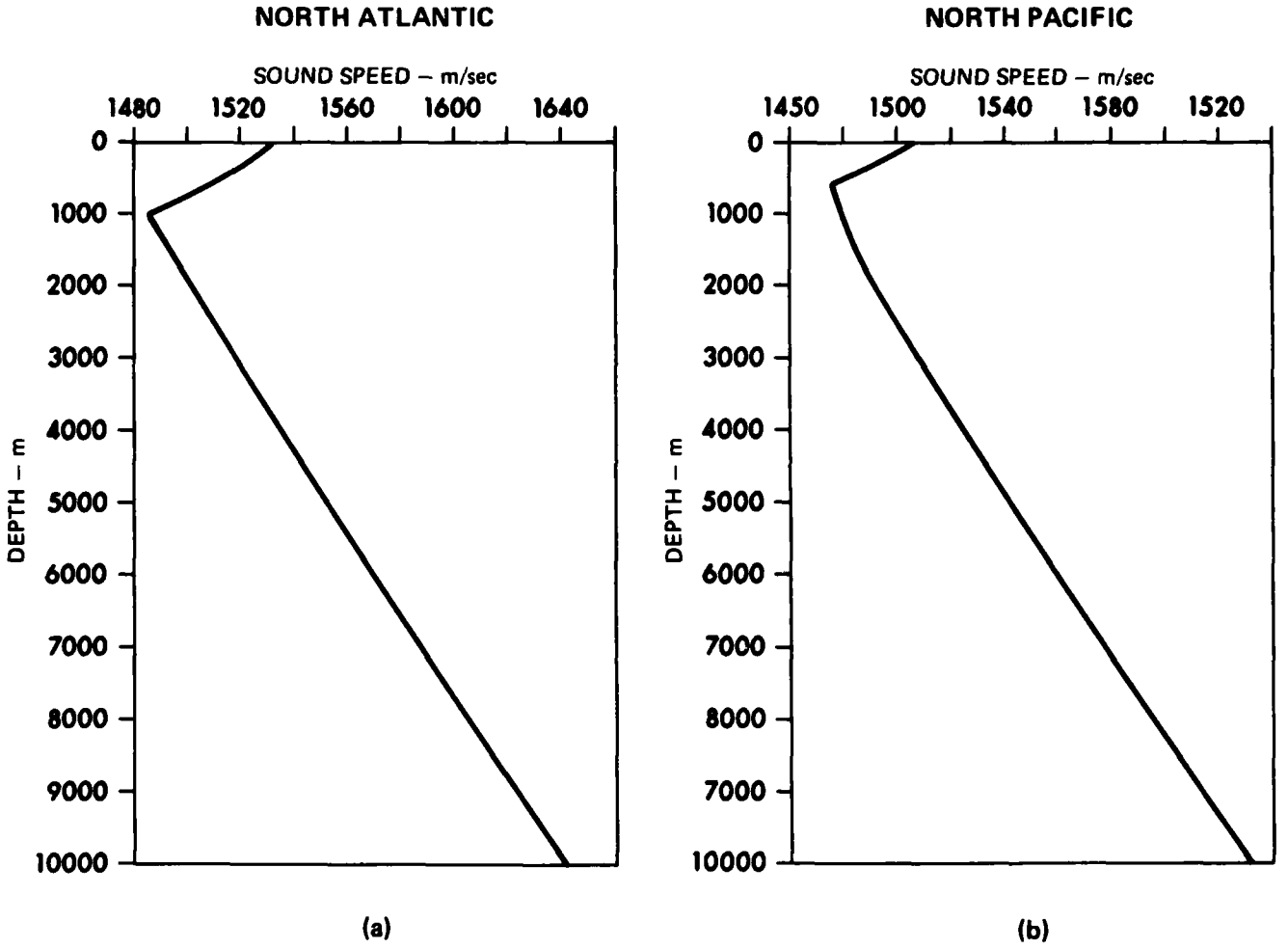

FIGURE 6
SOUND SPEED PROFILES USED FOR RAY TRACING CALCULATIONS

ARL:UT
AS-84-237
CLM - GA
4 - 2 - 84

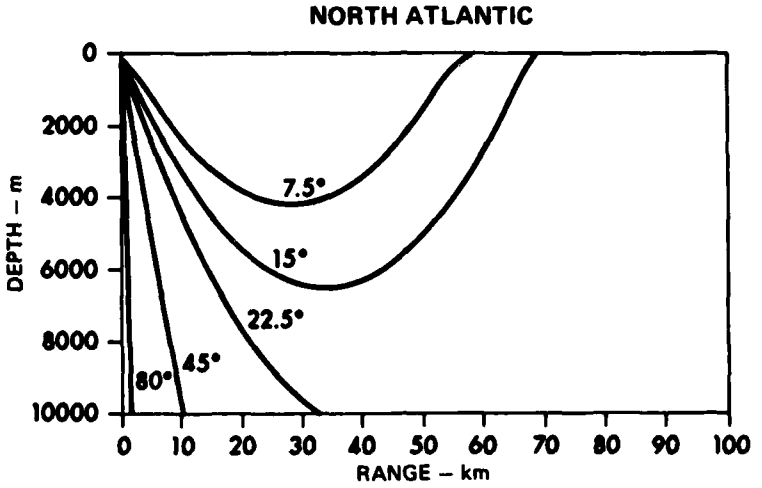

(a) z_0 = 200 m

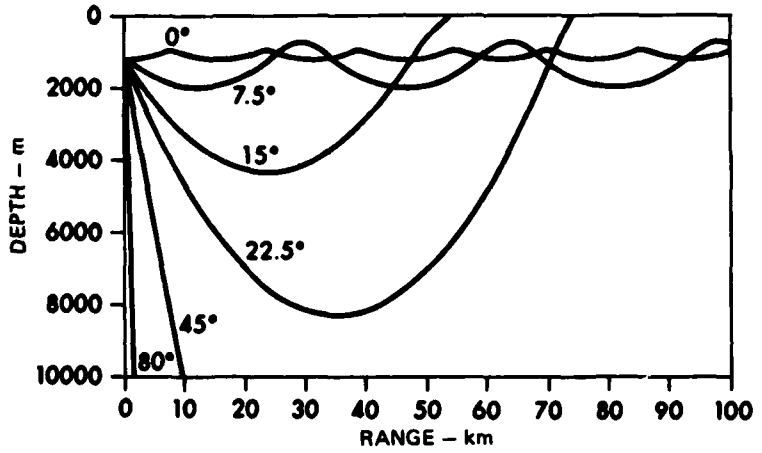

(b) z_0 = 1200 m

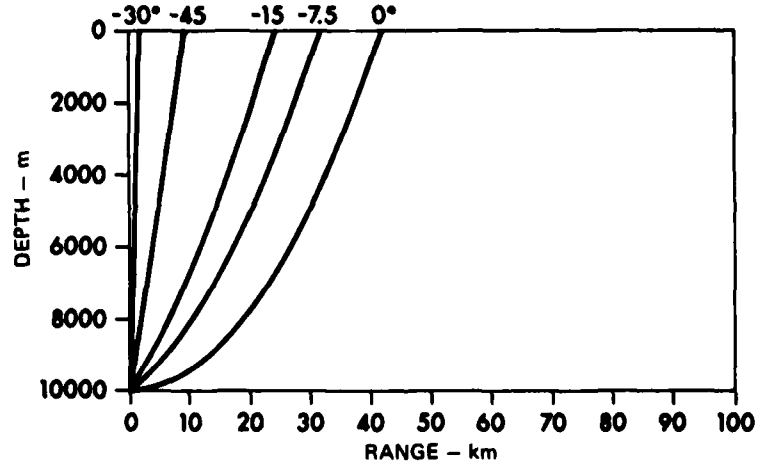

(c) z_0 = 10000 m

ARL:UT
AS-84-239
CLM - GA
4 - 2 - 84

FIGURE 7
NORTH ATLANTIC RAY PATHS

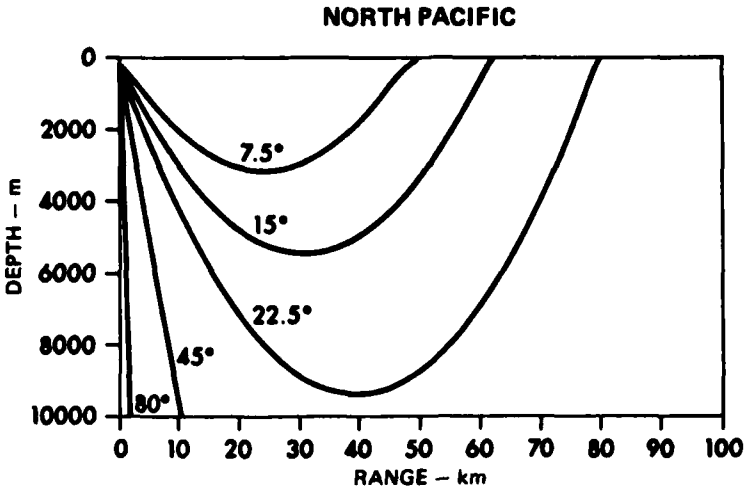

(a) z_0 = 200 m

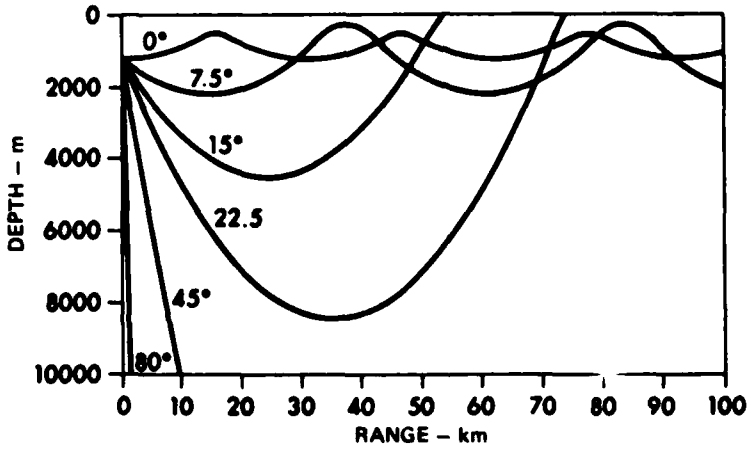

(b) z_0 = 1200 m

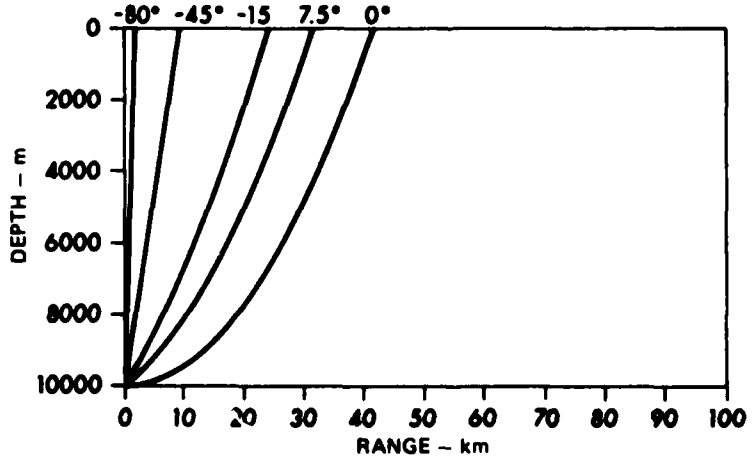

(c) z_0 = 10000 m

ARL:UT
AS-84-238
CLM · GA
4 · 2 · 84

FIGURE 8
NORTH PACIFIC RAY PATHS

NORTH ATLANTIC

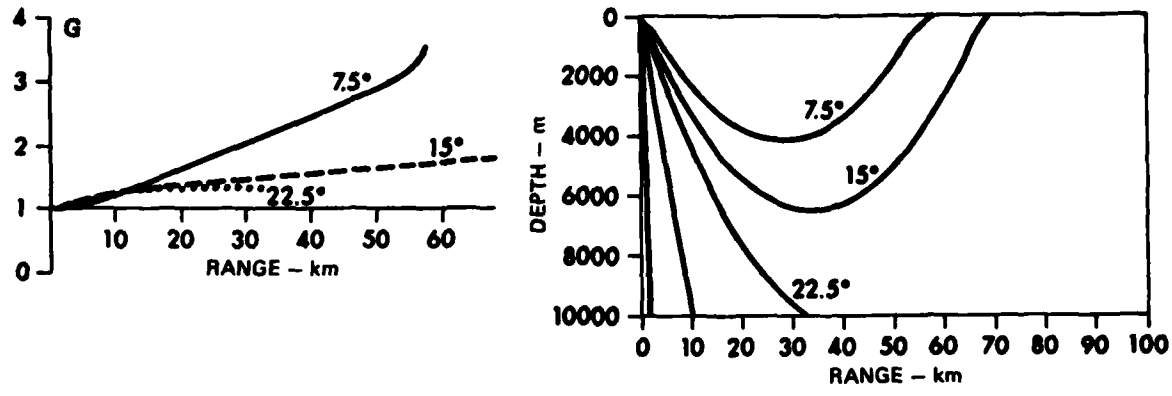

(a) z_0 = 200 m

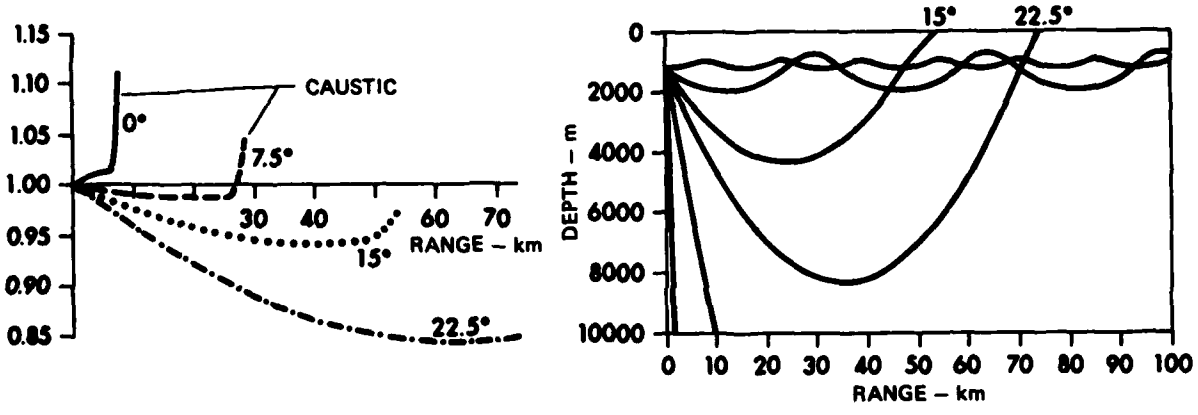

(b) z_0 = 1200 m

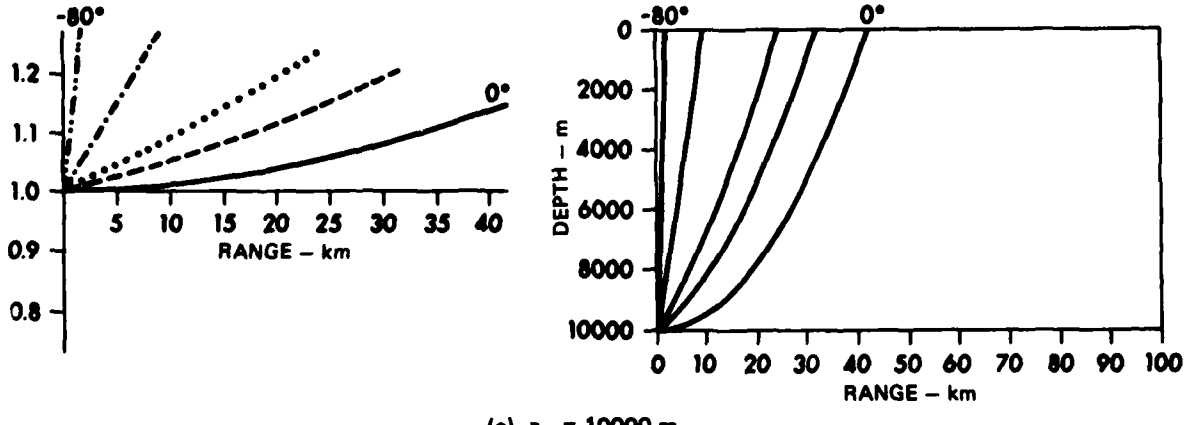

(c) z_0 = 10000 m

FIGURE 9
PLOT OF G versus HORIZONTAL RANGE x, FOR RAY PATHS IN NORTH ATLANTIC MODEL

ARL:UT
AS-84-240
CLM - GA
4 - 2 - 84

(Although ray tube areas could be computed for the surface reflected ray, the phase change on reflection makes it necessary to restart the nonlinear distortion calculation from this point.)

(b) The ray reaches the ocean bottom.

(Again, continuation of the G calculation beyond this point has no meaning, except in the special case where the bottom reflection coefficient is equal to 1.)

(c) The ray tube area approaches zero.

(At the caustic, the ray tube area vanishes but G remains finite. An asymptotic analysis of the behavior of G in this region appears in section IV-F below.)

The program which calculates G stops as soon as one of these criteria is met.

Corresponding ray paths for the representative North Pacific profile are shown in Fig. 8. The general pattern is similar to that of Fig. 7. Again, there are two channeled rays shown in Fig. 8(b); the cycle lengths and ranges to caustic formation are somewhat larger than for the corresponding rays in Fig. 7(b).

In the next three subsections we present a discussion of the numerical G values computed along these ray paths.

D. Numerical Results for the Distance Modification Factor G: Variation with Horizontal Range

Figures 9 and 10 show how the distance modification factor G varies along each ray path, for the North Atlantic and North Pacific cases respectively. To interpret these results, we recall the definition of G. Given a uniform ocean which matches the real ocean near the source, and given the same source level, sG is the propagation distance required to reproduce the signal distortion found at distance s along a ray path in the real ocean. Thus G values greater than 1 indicate enhanced

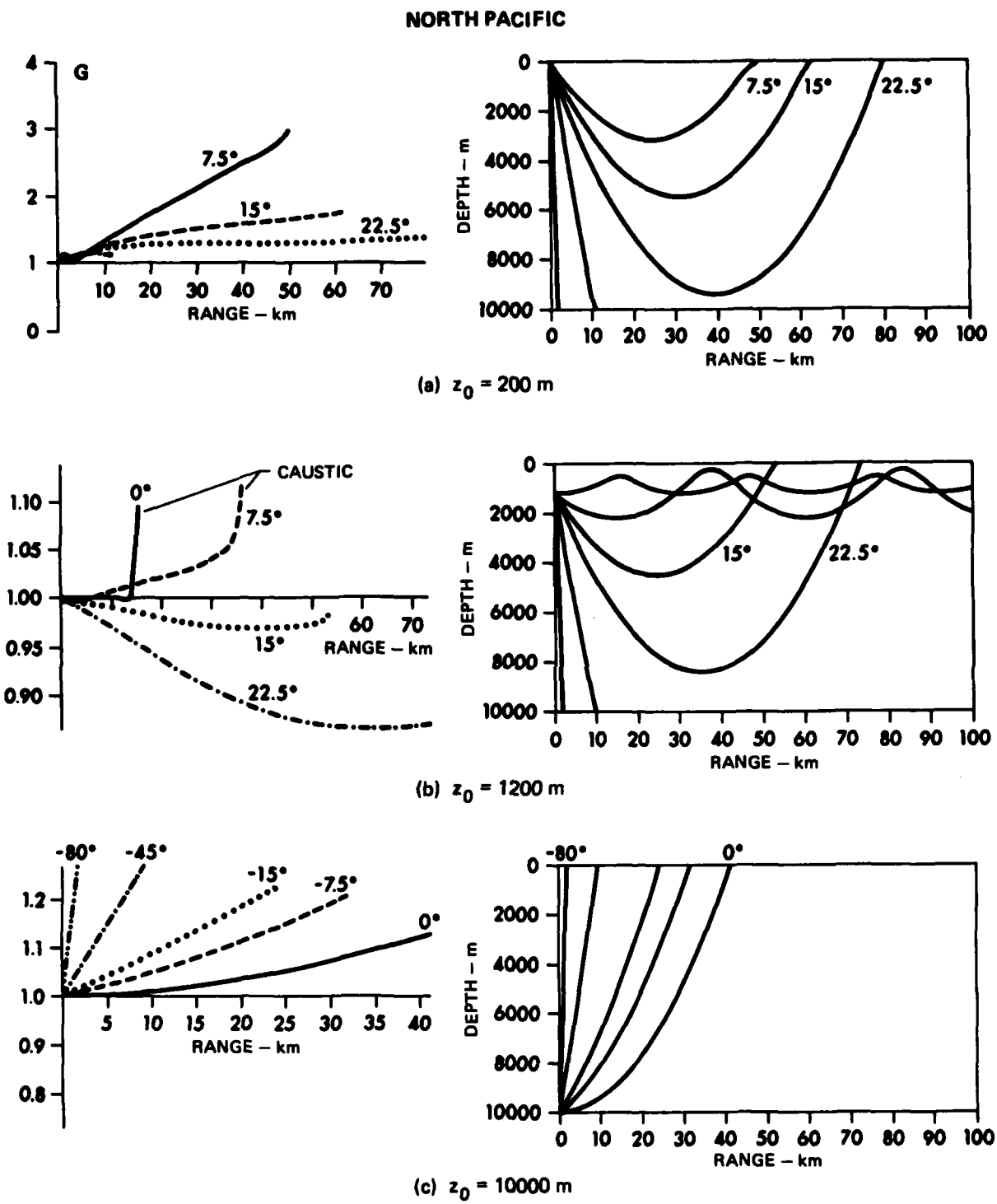

FIGURE 10
PLOT OF G versus HORIZONTAL RANGE x, FOR RAY PATHS IN NORTH PACIFIC MODEL

ARL:UT
AS-84-236
CLM - GA
4 - 2 - 84

nonlinear distortion, and vice versa. (Note that throughout this report, dissipative phenomena--except at shocks--are neglected: in reality a signal propagating along a ray path of increased length would suffer additional attenuation and dispersion, which are being left out of account for the present.*)

We first examine Fig. 9, which presents results for the North Atlantic profile. (The results for the North Pacific are qualitatively similar--see Fig. 10.) Three source depths are used: (a) 200 m, (b) 1200 m, and (c) 10,000 m, corresponding to the ray paths in Figs. 7 and 8. We shall see that provided the sound speed continues to increase (or decrease) monotonically along the ray path, the variation of G follows the trends predicted by the theory of Section III. On the other hand, once dc/ds changes sign, G departs quite dramatically from the predictions of the asymptotic theory.

1. Source Depth 200 m

This case provides a good illustration of the departures mentioned above. Figure 9(a) shows G reaching a value of 3.5 as the shallowest ray (θ_o=7.5°) reaches the surface. The growth of G in this case is progressive, starting from a horizontal range of about 5 km which is the point at which the downward-going ray crosses the sound channel axis. A similar progressive growth in G may be seen along the θ_o=15° ray, although it is less pronounced (G reaches 1.8 at the surface). Rays launched more steeply downwards are cut short by the bottom, but would presumably continue this trend in an ocean of infinite depth (the present model ocean is 10,000 m deep).

Two principal observations may be drawn from Fig. 9(a). First, shallow angle rays launched towards the sound channel axis can acquire sufficient focusing, by the time they cross the axis, that quite large G values accumulate during subsequent propagation back to the source depth. This is a consequence of the reduction in ray tube area S(s) relative to spherical spreading.

* The validity of the lossless fluid assumption, for typical underwater shock pulse waveforms with various initial timescales, is being assessed (as a function of propagation distance) as part of a follow-on to the present investigation.

The second observation relates to rays launched more steeply towards the channel axis (e.g., in Fig. 9(a), the 22.5° ray), which penetrate beyond the axis into regions of relatively high sound speed. Somewhat surprisingly, in this case the initial focusing over the first few hundred meters (between the source and the sound channel axis) is sufficient to cause G to go on increasing for several thousand meters more, despite the defocusing effect of a monotonically increasing sound speed as the ray propagates downwards.

2. Source Depth 1200 m

In this case the source is just below the sound channel axis. Rays launched downwards therefore experience a progressive increase in sound speed until a vertex is reached. According to the asymptotic theory of Section III, which predicts $G \propto (c/c_o)^{-1.5}$, G is expected to decrease slowly from its initial value of one, and this is observed in Fig. 9(b) (θ_o=7.5°, 15°, 22.5°). Beyond the vertex the asymptotic theory offers no guidance; but the numerical results in Fig. 9(b) show a flattening off, followed by either a rapid increase as a caustic is approached (θ_o=0°, 7.5°), or a gentle upturn as the ray reaches the surface (θ_o=15°, 22.5°).

The variation of G near a caustic will be discussed further in subsection F below. Otherwise, the main conclusion drawn from Fig. 9(b)--and the similar results for the North Pacific profile in Fig. 10(b)--is that G values for sources close to the sound channel axis remain in the range 0.85 to 1.0, caustic regions excepted.

3. Source Depth 10,000 m

The rays launched from the deepest source location experience a monotonic decrease in sound speed ($dc/ds < 0$) over the first 90 percent or more of their path to the surface. The asymptotic theory of Section III applies to this region, and the calculated values of G in Fig. 9(c) show the predicted behavior all the way up to the sound channel axis (depth 1000 m). Values of G at this depth vary from 1.12 (θ_o=0) to 1.25 ($\theta_o \leq 45°$).

Beyond the sound channel axis, dc/ds changes sign and a one-to-one relation between G and c/c_o is no longer expected. Figure 9(c) shows that G actually continues to increase between the sound channel axis and the surface, maintaining the trend established over the earlier part of the propagation path.

Corresponding plots of G versus x for the same three source depths (z_o=200, 1200, 10,000 m) are shown in Figs. 10 (a,b,c) for the North Pacific profile. The same trends are observed as in Fig. 9, and the same conclusions apply. The main differences of detail occur with the caustic forming rays (z_o = 1200 m; θ_o = 0°, 7.5°), and these are discussed in subsection F which deals specifically with caustics.

E. Numerical Results for the Distance Modification Factor G: Relation between G and c/c_o

A major conclusion from the theoretical analysis in Section III is that under certain conditions--principally when ray angles are not too shallow and also dc/ds does not change sign--G is a function of c/c_o only. Some supporting evidence from the present numerical study has been discussed in the preceding paragraphs. We now test the theoretical conclusion directly using Figs. 11 through 13, which plot G versus c/c_o for each of the source depths in turn.

For the shallowest source location (z_o = 200 m), the rays travel only a short distance before dc/ds changes sign at the channel axis (z = 1000 m for the North Atlantic, or 600 m for the North Pacific model profile). The theory is therefore not severely tested in Fig. 11; the plots terminate on the axis, before G has changed significantly. Nevertheless the collapse of results for different launch angles (apart from the shallowest angles, θ_o=7.5° and 15°) is encouraging.

The collapse is next tested for rays launched from z_o = 1200 m, in Fig. 12. The dc/ds criterion terminates the plots at either the channel axis (when θ_o=0°), or the first vertex (θ_o=15°, 22.5°). The two steepest rays are terminated at 10,000 m depth, giving G=0.89. There is a definite tendency towards collapse on a c/c_o basis, with the main departures occurring as a vertex is approached.

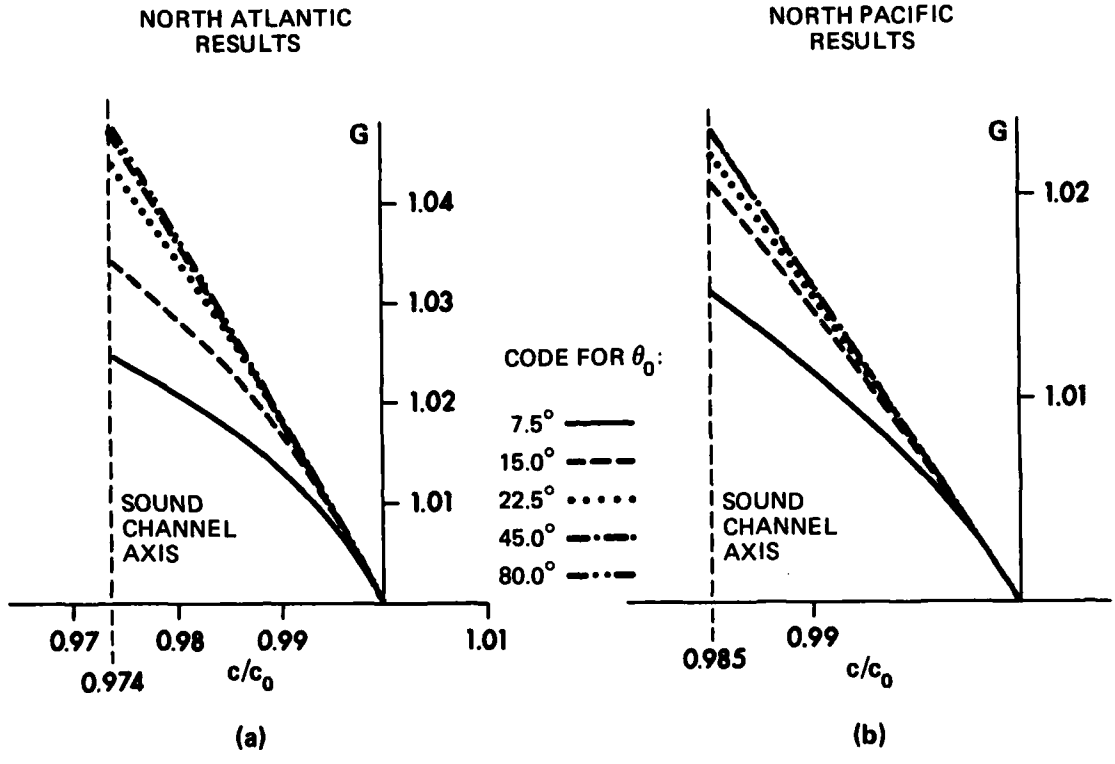

FIGURE 11
PLOT OF G versus SOUND SPEED RATIO (log-log SCALES): $z_0 = 200$ m

ARL:UT
AS-84-241
CLM - GA
4 - 2 - 84

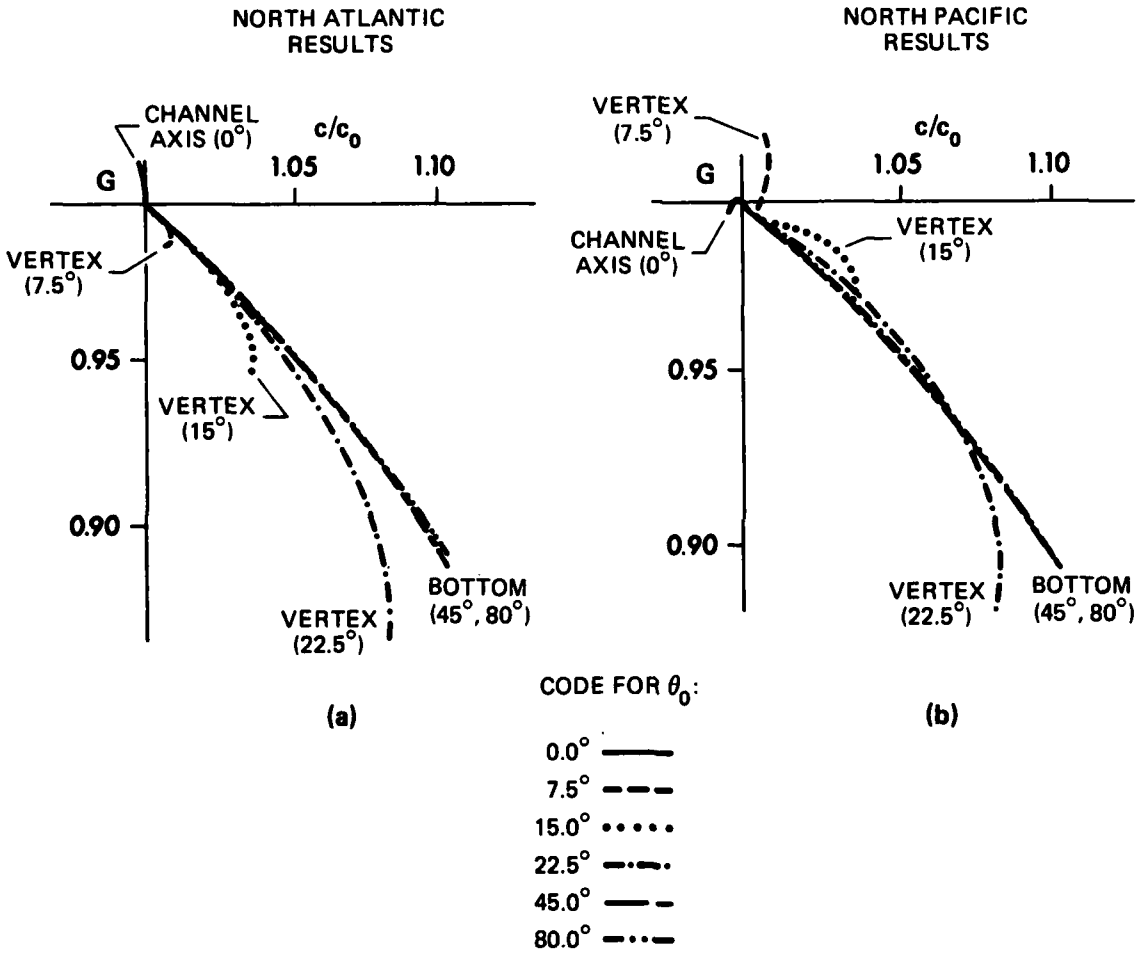

FIGURE 12
PLOT OF G versus SOUND SPEED RATIO (log-log SCALES): z_0 = 1200 m

ARL:UT
AS-84-242
CLM - GA
4 - 2 - 84

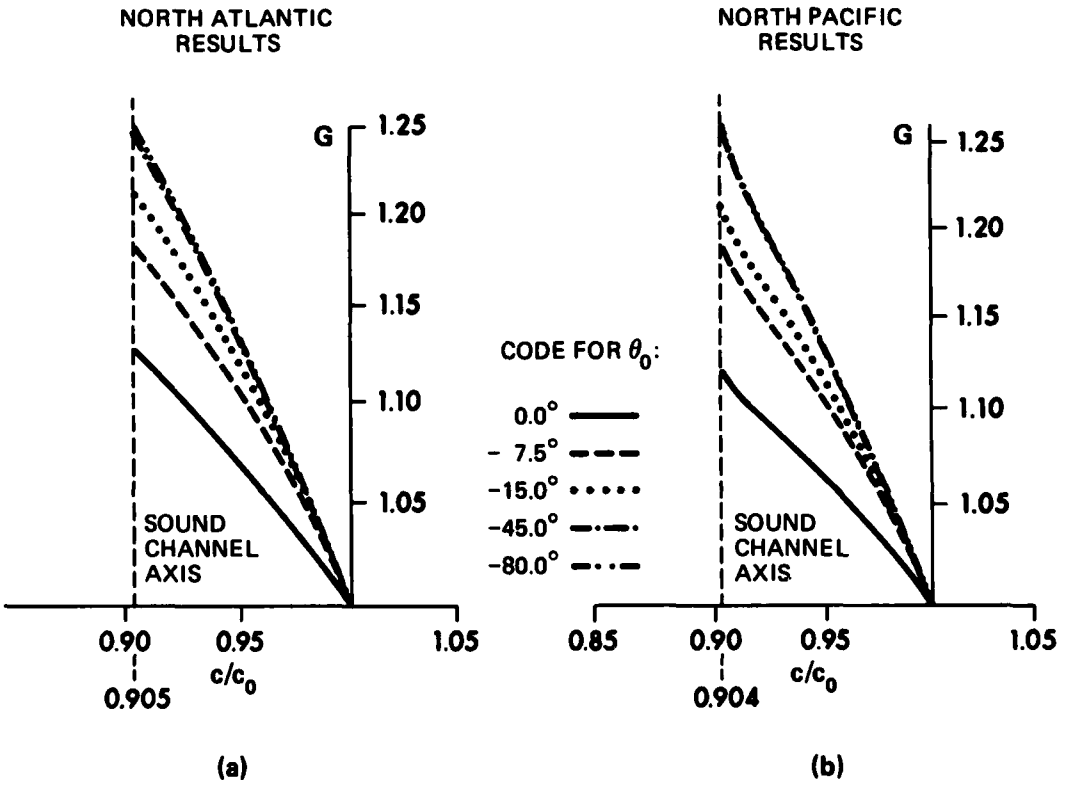

FIGURE 13
PLOT OF G versus SOUND SPEED RATIO (log-log SCALES): z_0 = 10,000 m

ARL:UT
AS-84-243
CLM - GA
4 - 2 - 84

Finally, Fig. 13 shows the bottom-launched ray results plotted in the same format. The plots in this case all terminate at the sound channel axis. At this point the spread in G values, across the launch angle range -15°to -80°, is only about 3 percent (North Atlantic profile) or 4 percent (North Pacific profile).

From these plots of G versus c/c_o we may deduce power laws of the form

$$G = (c/c_o)^{-m} \quad , \tag{25}$$

which give a fairly accurate description of the way the distance modification factor varies along rays which are not too near the horizontal. The values of the index m listed in Table IV represent an approximate straight line fit to the results for $\theta_o = \pm 80°$. They range between 1.05 and 2.3, as compared with the value 1.5 arrived at from an asymptotic analysis in Section III for an idealized ocean profile.

TABLE IV. INDEX m OBTAINED BY FITTING THE POWER LAW $G = (c/c_o)^{-m}$ TO THE CURVES IN FIGURES 11-13 (STEEP RAY LIMIT)

Figure No.	Index m	Depth range
11 (a)	1.75	200 m down to
11 (b)	1.55	sound channel axis
12 (a)	1.1	1200 m to 10,000 m
12 (b)	1.05	(downward propagation)
13 (a)	2.3	10,000 m to channel axis
13 (b)	2.3	(upward propagation)

A significant conclusion from the results presented in Figs. 11 through 13 is that an order of magnitude estimate of G is possible on the basis of c/c_o alone, provided the ray path is such that dc/ds does not change sign. The equation recommended for this purpose, namely

$$G = (c/c_o)^{-1.5} \quad , \tag{26}$$

is a compromise which covers the range of launch angles and source depths in Figs. 11 through 13; actual m values along the different rays vary from 0.9 to 2.3. Accordingly, Eq. (26) is expected to predict log G (and hence the reduced distance $\bar{x}$) within a factor of 2, under typical ocean conditions and without requiring detailed information on the ocean profile and ray path.

F. The Approach to a Caustic

A caustic is formed when neighboring rays cross; the ray tube area then vanishes, and according to geometric acoustics the intensity would be infinite. In the region within a wavelength or so of the caustic, this prediction is invalid. However, up to this region a marked increase in G is expected as the rate of nonlinear distortion accelerates along the converging ray tube.

Figure 14 shows two neighboring rays which intersect at range x_c, on the caustic. By simple geometry, we can relate the area of the converging wavefront to the launch angle derivative of the ray angle, $(d\theta/d\theta_o)$, evaluated at the caustic (subscript c).

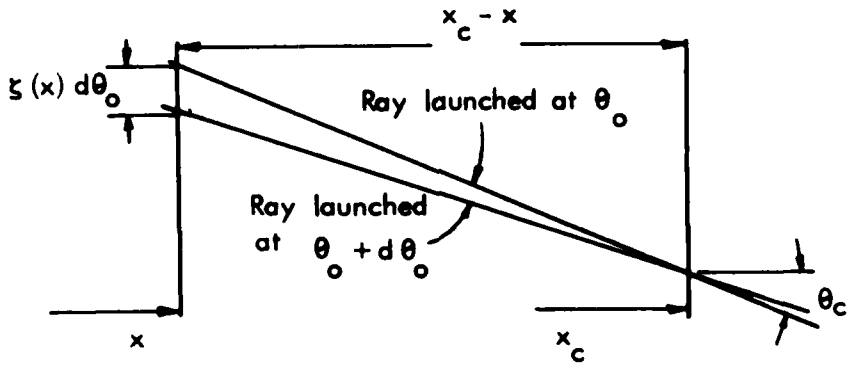

FIGURE 14
SKETCH SHOWING RAY TUBE CONVERGENCE AT A CAUSTIC

The resulting variation of G--which is dominated by the ray tube area convergence--follows from the analysis given below.

Appendix F gives the logarithm of G as an integral along the ray path,

$$\ln G(s) = F(s) = \int_0^s \left\{ A(s') - \frac{1}{s'} \right\} ds' \quad . \tag{27}$$

The quantity A(s) is related to the ray tube area S(s), and is defined by

$$A(s) = \lim_{s_o \to 0} \frac{1}{s_o} \left(\frac{S}{S_o} \right)^{-\frac{1}{2}} \frac{\alpha}{\alpha_o} \quad . \tag{28}$$

It is clear from Fig. 14 that as the caustic is approached (at $x=x_c$), the ray tube area varies as

$$S \sim (x_c - x) \qquad (x < x_c) \tag{29}$$

and that the other terms in the integral above may be regarded as constant in the neighborhood of the caustic. The change in F(s) between x and x_c follows as

$$\Delta F \simeq \int_x^{x_c} K(x_c - x')^{-\frac{1}{2}} \frac{dx'}{\cos\theta_c} \quad , \tag{30}$$

where K is the constant of proportionality in the asymptotic expression for A(s) deduced from Eqs. (28) and (29):

$$A(s) \simeq K(x_c - x)^{-\frac{1}{2}} \quad , \qquad (x < x_c) \quad . \tag{31}$$

Although the integrand in Eq. (30) is singular, the integral is finite and given by

$$\Delta F = \frac{2K}{\cos\theta_c} \; (x_c - x)^{\frac{1}{2}} \quad . \tag{32}$$

The constant K may be deduced from Eq. (28) and the ray tube area relation

$$\frac{S}{S_o} = \frac{x\zeta}{s_o^2} \frac{\cos\theta}{\cos\theta_o} \quad , \tag{33}$$

if we make use of the asymptotic result

$$\zeta \simeq (\zeta_x)_c (x - x_c) \qquad (\zeta_c = 0 \text{ by definition})$$

$$= \frac{\partial}{\partial \theta_o} (z_x)\Big|_{x=x_c} \cdot (x - x_c)$$

$$= \frac{\partial \tan\theta}{\zeta \theta_o}\Big|_{x=x_c} \cdot (x - x_c)$$

$$= \sec^2 \theta_c \cdot \left(\frac{d\theta}{d\theta_o}\right)_c (x - x_c) \quad . \tag{34}$$

The value of K thus obtained is

$$K = \frac{\alpha_c}{\alpha_o} (\cos\theta \cos\theta_c)^{1/2} \left(-\frac{d\theta}{d\theta_o}\right)_c^{-1/2} x_c^{-1/2} \quad , \tag{35}$$

which when combined with Eq. (32) above gives

$$\Delta F \simeq 2 \frac{\alpha_c}{\alpha_o} \left(\frac{c_c}{c_o}\right)^{1/2} \left(-\frac{d\theta}{d\theta_o}\right)_c^{-1/2} \left(\frac{x_c - x}{x_c}\right)^{1/2} \quad . \tag{36}$$

For purposes of rough estimation the factor $(\alpha_c/\alpha_o)(c_c/c_o)^{1/2}$ may be replaced by 1. Then we find, on putting $x = 0.9\, x_c$, that over the final 10 percent of the horizontal range up to the caustic,* G increases by a factor $\exp[\Delta F(10\%)]$ defined as follows:

$$G(x_c)/G(0.9x_c) = \exp[\Delta F(10\%)] \quad , \tag{37}$$

where

$$\Delta F(10\%) \simeq \frac{2}{10^{1/2}} \left(-\frac{d\theta}{d\theta_o}\right)_c^{-1/2} \quad . \tag{38}$$

* It is assumed that negligible ray bending occurs over the final 10 percent of the range, so that the asymptotic relation (36) may be applied. For the relevant ray paths, see Figs. 9(b) and 10(b).

The numerical examples discussed in this report include four rays which form caustics. These are the rays launched at θ_o values of 0° and 7.5°, from a depth of 1200 m (both ocean profiles). For these four rays, Table V lists values of the following parameters:

(a) The horizontal range x_c at which the caustic is formed.

(b) The ray angle θ_c at the caustic.

(c) The derivative $(-d\theta/d\theta_o)_c$, evaluated from the relation

$$\left(\frac{d\theta}{d\theta_o}\right)_c = (\xi_x \cos^2\theta)_c \tag{39}$$

which follows from Eq. (34).

(d) The factor $\exp[\Delta F(10\%)]$ by which G(x) is estimated to increase between 0.9 x_c and x_c, evaluated from Eq. (38) above.

TABLE V. RAY PATH PARAMETERS EVALUATED AT THE CAUSTIC

Results for two different ocean profiles (as in Table III). The source is located near the sound channel axis (source depth = 1200 m).

θ_o (deg)	x_c (km)	θ_c (deg)	$(-d\theta/d\theta_o)_c$	Profile	$\frac{G(x_c)}{G(0.9x_c)}$
0	7·7605	-0.01	3.6747	N. Atlantic	1.39
7.5	28·687	-1.07	7.2158	N. Atlantic	1.27
0	15·4905	0.15	5.3047	N. Pacific	1.32
7.5	36·730	-1.14	6.4757	N. Pacific	1.28

The range derivative ξ_x required for the last two table entries is provided at each point along the ray path by the MEDUSA program, and values at the caustic have been deduced by linear interpolation.

It is interesting to note, from Table V, that $(-d\theta/d\theta_o)_c$ is significantly greater than one (of order 5) for the examples studied. The larger this ratio becomes, the smaller the increase in G associated with convergence of the ray tube, for a given starting value of x/x_c (assumed close to one).

The final column in Table V shows that the predicted increase in G, between $0.9\,x_c$ and the caustic location x_c, is of order 30 percent. The numerically calculated increases, shown in the plots of G versus x (see Figs. 9(b) and 10(b) discussed earlier), are considerably less, of order 5 to 10 percent. The reason is that the numerical plots are terminated at the last step before the caustic is reached. In order to continue the plots up to the caustic, it would be necessary to modify the MEDUSA ray tracing program to locate the caustic automatically.

V. CONCLUSIONS

The principal conclusions from the present study of nonlinear propagation in an inhomogeneous ocean are as follows.

(1) An analytical model for finite-amplitude sound propagation in an inhomogeneous ocean has been set up, based on ray theory combined with the weak-shock approximation.

(2) Within the framework of the model, separation has been achieved between the nonlinear aspects of the problem and the purely linear aspects, by defining a distance modification factor for nonlinear propagation.

(3) The distance modification factor G defines the equivalent propagation distance in a uniform ocean,

$$s_{equiv} = sG \ ,$$

which reproduces the nonlinear distortion found in the inhomogeneous case under the same source conditions.

(4) An asymptotic theory, valid for ray paths along which dc/ds does not change sign, predicts that G is principally a function of the local sound speed ratio c/c_o.

(5) A numerical scheme has been developed for calculating G. Input data for the calculation is provided by a ray tracing program developed at ARL:UT. The scheme has been verified for an idealized ocean profile with a constant sound speed gradient, by comparing the results with an exact analytic solution for G which has been developed for this case.

(6) The distance modification factor has been evaluated numerically, for two typical deep ocean profiles and several combinations of source depth and ray launch angle. Up to the point on each ray path where

dc/ds changes sign, the asymptotic theory is found to yield an approximate collapse of all the results in terms of c/c_o.

(7) Some of the rays in the numerical study exhibit caustic formation. The increase in G which occurs, as a ray approaches a caustic, has been predicted asymptotically.

(8) The range limitations on weak-shock theory are being explored in a separate study, with particular reference to transient pulses in a real ocean with chemical relaxation effects.

APPENDIX A

LIST OF SYMBOLS

A	function of s, Eq. (F-2)
a	profile constant, Eq. (24) and Appendices D, E; constant in empirical Eq. (C-3) for β
B	function of s, Eq. (F-13)
b	profile constant, Appendix D; constant in empirical Eq. (C-4) for β
C	constant, Eq. (D-26)
C_P	constant-pressure specific heat
c	sound speed
F	function of s, Eq. (F-8); function of (P,T,S), Eq. (B-5)
f	general function; derivative of F(s), Appendix F
G	distance modification factor for nonlinear propagation in an inhomogeneous ocean, Eq. (9)
K	constant in asymptotic A(s) expression, Eq. (31)
m	power law index, Eq. (25); profile index, Eq. (D-13)
N_c, N_α	number of points used to define numerical profiles of c(z), α(z)
n	power law index, Eq. (12)
P	hydrostatic pressure (kgf/cm^2)
P'	gauge pressure
p	acoustic pressure
p	reduced pressure
S	ray tube area; salinity ($^o/oo$)
s	distance along ray from source
s_o	reference distance close to source
T	temperature (°C)
t	time
t'	retarded time for linear waves, Eq. (2)
W	function of s, Eq. (F-1)

x	horizontal range
$\bar{x}$	reduced distance, Eq. (6)
z	depth below surface
z_o	source depth
α	$\beta(\rho c^5)^{-1/2}$
α_T	thermal expansion coefficient
β	nonlinearity parameter
ζ	launch angle derivative of $z(\theta_o,x)$ on ray, Eq. (11)
θ	ray angle (downwards from horizontal)
θ_o	launch angle
λ	$\cos\theta_o$, Appendix D; function of (T,S), Eq. (B-4)
ξ	launch angle derivative of $x(\theta_o,z)$ on ray, Eq. (10)
ρ	fluid density
σ	dimensionless sound speed variation, Appendix D
τ	nonlinear retarded time variable
ϕ	latitude angle

Subscripts

o	value at source
c	value at caustic

APPENDIX B

FORMULAS FOR HYDROSTATIC PRESSURE, DENSITY, SOUND SPEED AND NONLINEARITY PARAMETER IN THE OCEAN.

In the expressions below, P is the hydrostatic pressure in kgf/cm^2 (1 kgf/cm^2 = 0.980665 bar). Gauge pressure relative to 1 atm is denoted by

$$P' = P - 1.033 \quad . \tag{B-1}$$

Also T is the temperature in °C, and S is the salinity in °/oo.

Hydrostatic Pressure

Leroy's formula[5] for hydrostatic pressure P as a function of depth z (in m) and latitude ϕ is as follows:

$$P = 1.04 + 0.102506\,(1 + 0.00528 \sin^2\phi)z + 2.524E\text{-}07\, z^2 \quad . \tag{B-2}$$

This formula is supposed to be valid for all oceans except the Black Sea and the Baltic.

Density (P,T,S)

The density ρ (in kg/m^3) is given by Eckart's formula[6]

$$\rho = \frac{999.97}{0.698 + \lambda/F} \quad , \tag{B-3}$$

where

$$\lambda = 1779.5 + 11.25\,T - 0.0745\,T^2 - (3.80 + 0.01\,T)S \quad , \tag{B-4}$$

and

$$F = 5890 + 38\,T - 0.375\,T^2 + 3\,S + 0.96784\,P \quad . \tag{B-5}$$

Wilson and Bradley[7] have given an alternative formula, based on more recent data, which will be compared with Eq. (B-3) in the next phase of this study.

Sound Speed c(P,T,S)

The sound speed c (in m/sec) is given by Wilson's formula[8]

$$c = 1449.14 + V_P + V_T + V_S + V_{STP} \tag{B-6}$$

in which the V's are polynomials of up to 4th degree in the indicated variables. Explicit expressions are given in Ref. 8.

Nonlinearity Parameter (P,T,S)

The nonlinearity parameter β is given by Carlton's formula[9]

$$\begin{aligned}\beta = {} & 3.3685 + 9.874\text{E-}07\ S^3 \\ & + 7.799\text{E-}06\ T^3 + 1.027\text{E-}03\ P' \\ & - 2.276\text{E-}10\ P'^3 + 5.429\text{E-}04\ ST \\ & - 8.641\text{E-}07\ STP' - 1.542\text{E-}05\ ST^2 \\ & + 1.620\text{E-}08\ T^3P' \ . \end{aligned} \qquad \text{(B-7)}$$

APPENDIX C

APPROXIMATE RELATIONS FOR α, β, AND DENSITY ρ IN SEAWATER

In this Appendix we examine the validity of the power law approximation for α in terms of sound speed, Eq. (12). We also show that the acoustic properties (α,β,ρ) in seawater may be quite accurately expressed in terms of just two variables, sound speed and temperature, rather than the usual three (temperature, pressure,and salinity). Finally, the relation for the nonlinearity parameter β used by Petukhov and Fridman[4] is shown to be inaccurate, and an alternative relation of similar form is given.

Power Law Relation between α and Sound Speed

In Section III.B, the relation

$$\frac{\alpha}{\alpha_o} = \left(\frac{c}{c_o}\right)^{-n} \qquad \text{(C-1)}$$

was proposed. Here α denotes the product $\beta(\rho c^5)^{-1/2}$, and clearly must depend in general on two other variables (e.g., pressure and salinity) besides the sound speed. Nevertheless Eq. (C-1) provides a first approximation to the actual variation of α with depth in the ocean, as we shall show here.

Values of α computed from the formulas given in Appendix B are plotted against the sound speed in Figs. C1 through C3. Isotherms are the gently sloping curves marked T=0, 10, 20 (degrees C) at their left ends, respectively. Isobars are the steeply sloping curves marked P=1,200,400, . . . at their upper ends, respectively. The reference value used for normalization corresponds to (10°C, 1 bar, 35°/oo). Because of the log-log scale, any power law of the form (C-1) will appear as a straight line on the graph.

Below the first 200 m in a typical deep ocean profile, e.g.,the North Pacific profile of Fig. 4, the temperature falls relatively rapidly from around 10°C near the surface to 2-3°C at 1-2 km depth. Below 2 km the temperature remains almost constant. The corresponding variation of with depth may thus be deduced from Fig. C1, if we assume a constant salinity of S=35°/oo. The depth profile can be traced on Fig. C1 by noting that the pressure (in bars) is approximately one-tenth of the depth (in meters).

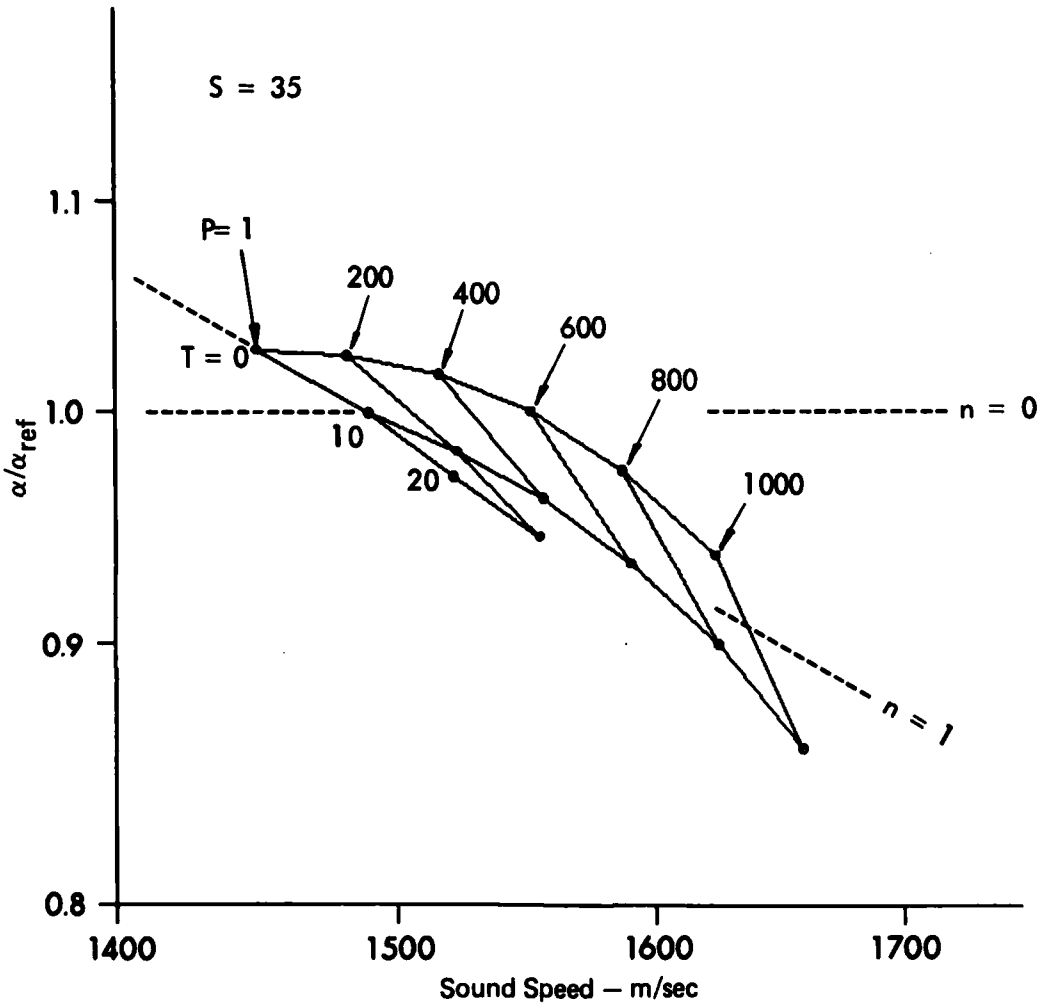

FIGURE C-1
α/α_{ref} versus c (LOG-LOG SCALES), FOR SEAWATER WITH SALINITY S = 35‰

ARL:UT
AS-84-497
DTB - GA
6 - 11 - 84

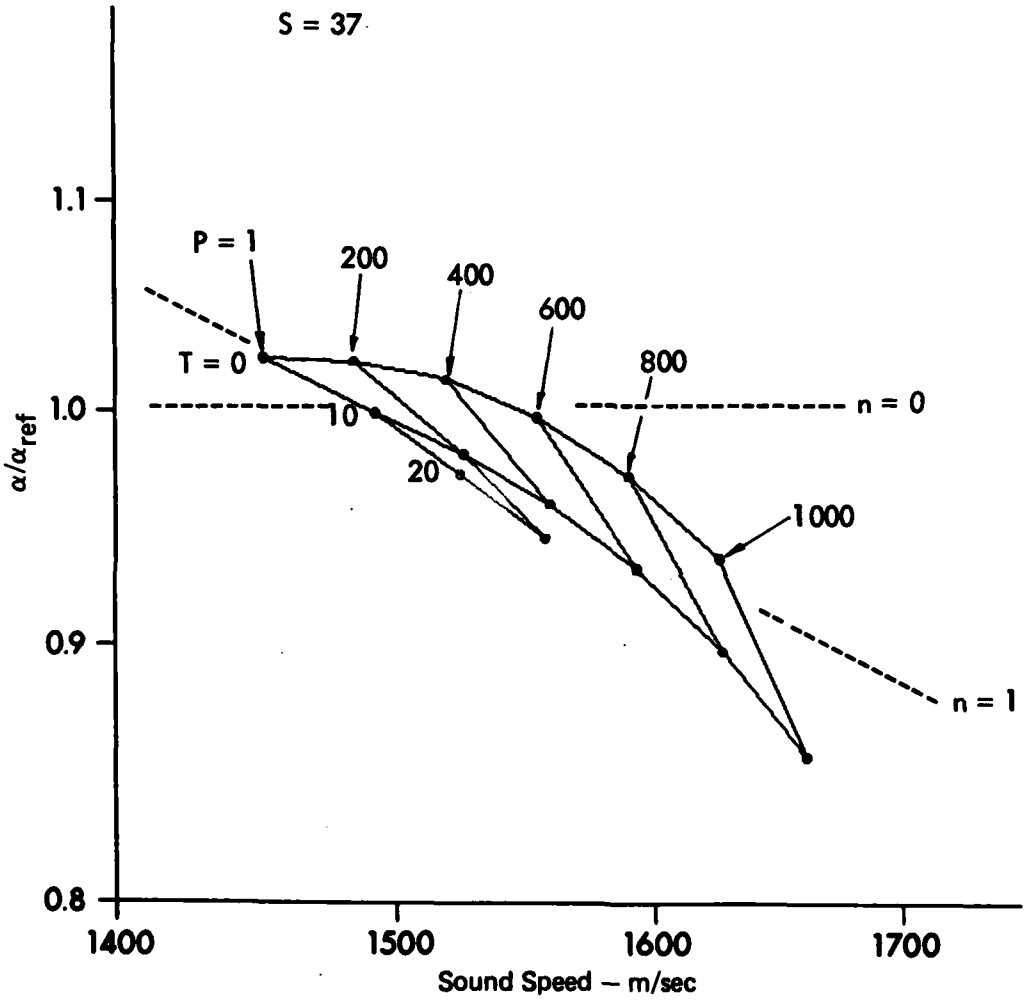

FIGURE C-2
α/α_{ref} versus c (LOG-LOG SCALES), FOR SEAWATER WITH SALINITY S = 37‰

ARL:UT
AS-84-498
DTB - GA
6-11-84

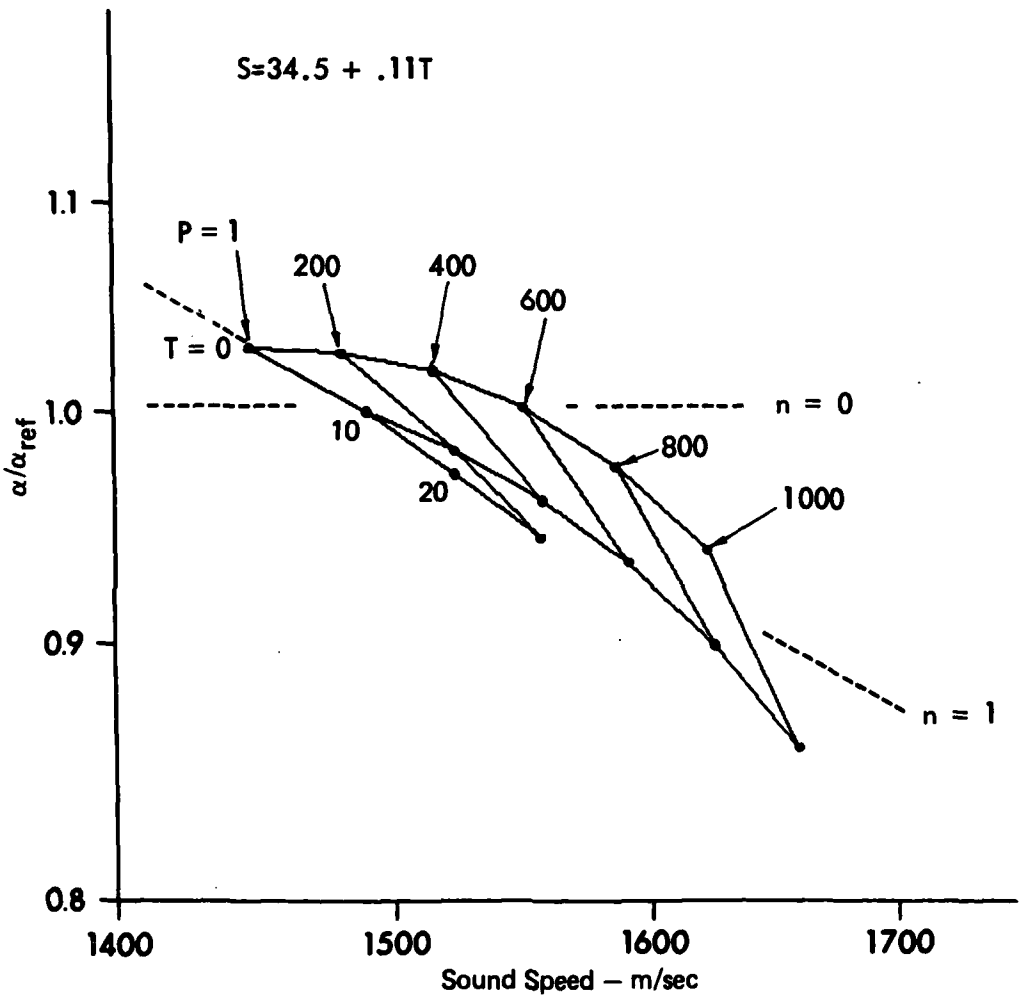

FIGURE C-3
α/α_{ref} versus c (LOG-LOG SCALES), FOR SEAWATER WITH SALINITY S = 34.5 + 0.11 T‰

ARL:UT
AS-84-499
DTB - GA
6 - 11 - 84

The resulting trace follows quite closely the line marked n = 1 in Fig. C1. A similar result is obtained by tracing the North Atlantic profiles of Fig. 4 onto Fig. C3, which incorporates an appropriate temperature-salinity relation.

We conclude that the power law Eq. (C-1), with n=1, provides a reasonably accurate model of the depth dependence of α suitable for analytical studies. Under certain restricted conditions a different index may be preferred, however. For example, at 0°C and depths less than 4 km, n=0 is more accurate.

Acoustic Properties as Functions of Sound Speed and Temperature

In Fig. C4, the density of seawater is plotted against sound speed. The same grid of temperature and pressure values has been used as in the previous three figures, although the constant-pressure lines are not drawn. Furthermore the grid has been evaluated for four different salinity values (S=34, 35, 36, 37 °/oo), although again for clarity these are marked only once.

The conclusion drawn from Fig. C4 is that the density of seawater may be determined quite accurately over a realistic salinity range from a knowledge of the sound speed and temperature, without recourse to a third parameter (e.g., pressure or salinity).

Figure C5 shows that a similar collapse along lines T=const. occurs for the nonlinearity parameter β, over the same range of salinity. It follows that a knowledge of (c,T) in the ocean is sufficient to estimate the important remaining acoustic properties β (or α) and ρ.

Empirical Relation between Nonlinearity Parameter and Characteristic Impedance

An expression for the nonlinearity parameter of any inert fluid, in terms of other thermodynamic derivatives, is

$$\beta = 1 + \rho c \left[\left(\frac{\partial c}{\partial P}\right)_T + \frac{\alpha_T T}{\rho C_P} \left(\frac{\partial c}{\partial T}\right)_P \right]. \qquad \text{(C-2)}$$

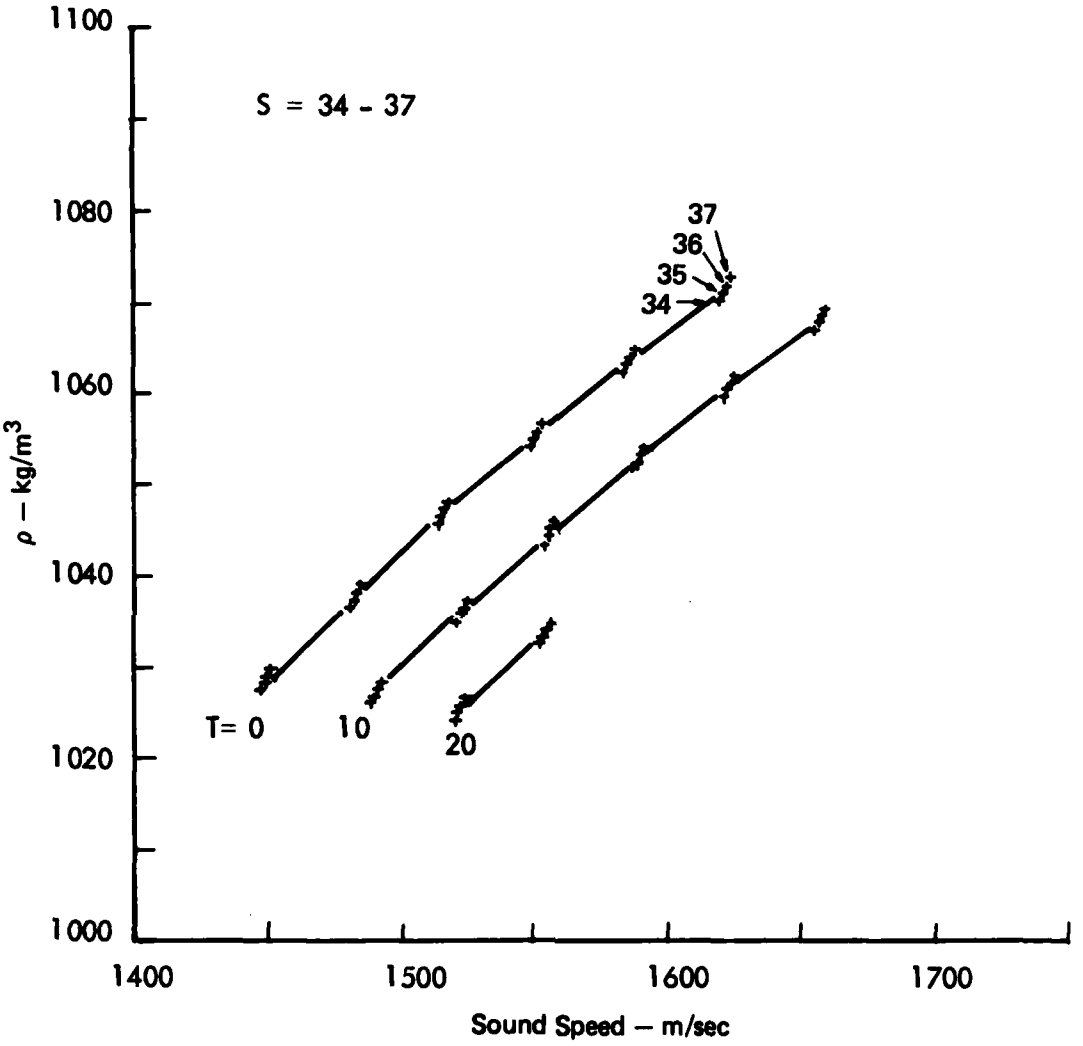

FIGURE C-4
DENSITY ρ versus c, FOR SEAWATER WITH SALINITY S = 34 to 37‰

ARL:UT
AS-84-500
DTB - GA
6-11-84

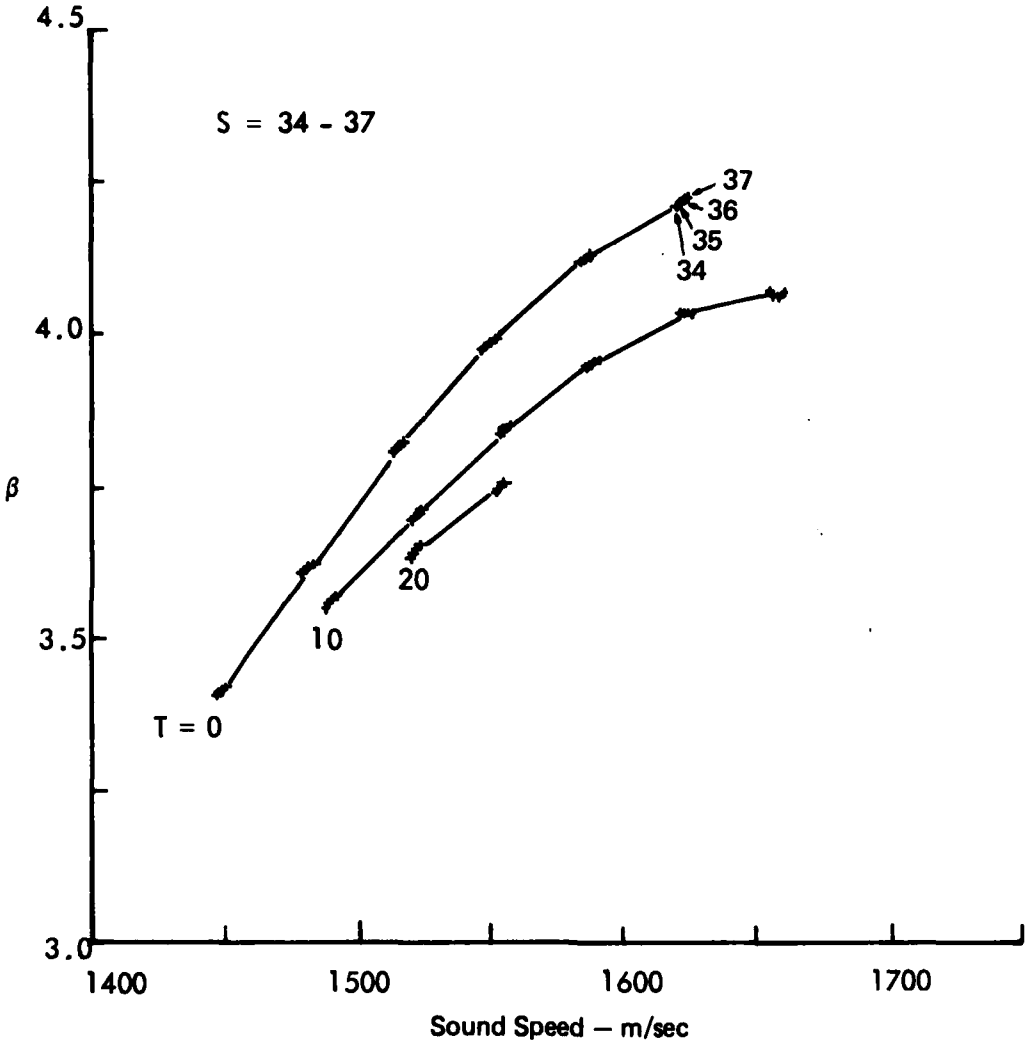

FIGURE C-5
NONLINEARITY PARAMETER β versus c, FOR SEAWATER WITH SALINITY S = 34 to 37‰

ARL:UT
AS-84-501
DTB - GA
6 - 11 - 84

Here α_T is the coefficient of thermal expansion, and C_p is the constant-pressure specific heat.

Guided by Eq. (C-2), Petukhov and Fridman[4] have proposed that the variation of β in seawater be estimated from

$$\beta = 1 + \rho c a \qquad (a = \text{const.}) \ , \tag{C-3}$$

which amounts to treating the bracketed factor in Eq. (C-2) as a constant.

Figures C6 and C7 show β plotted against ρc (again using the formulas in Appendix B), for two different salinity values. Evidently this presentation yields quite an accurate single-line collapse, for pressures and temperatures in the range P = 1-200 bar, T=0-20°C. However, Eq. (C-3) as it stands does not fit the data at all closely; it predicts the lines marked (a) in Figs. C6 and C7. (The constant a has been chosen to give the correct value of β at P = 1 bar, T=10°C).

A much better fit to the data, for typical ocean conditions, is given by

$$\beta = -2 + \rho c b \qquad (b = \text{const.}) \ . \tag{C-4}$$

Equation (C-4) is represented by the lines marked (b) in Figs. C6 and C7. A single value of the constant,

$$b = 3{\cdot}63 \cdot 10^{-6} \ m^2 s/kg \ , \tag{C-5}$$

has been used for each salinity.

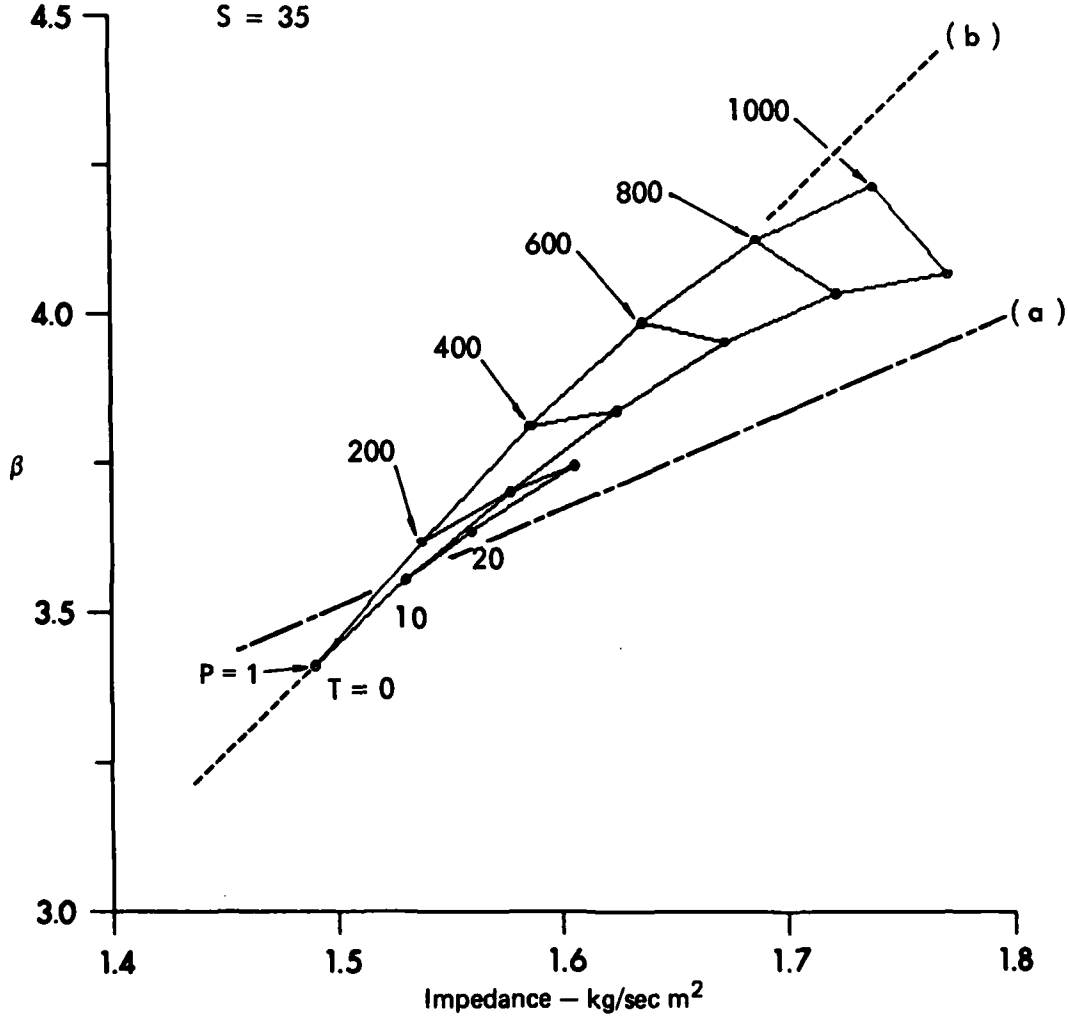

FIGURE C-6
β versus CHARACTERISTIC IMPEDANCE ρc, FOR SEAWATER WITH SALINITY S = 34‰

ARL:UT
AS-84-502
DTB - GA
6 - 11 - 84

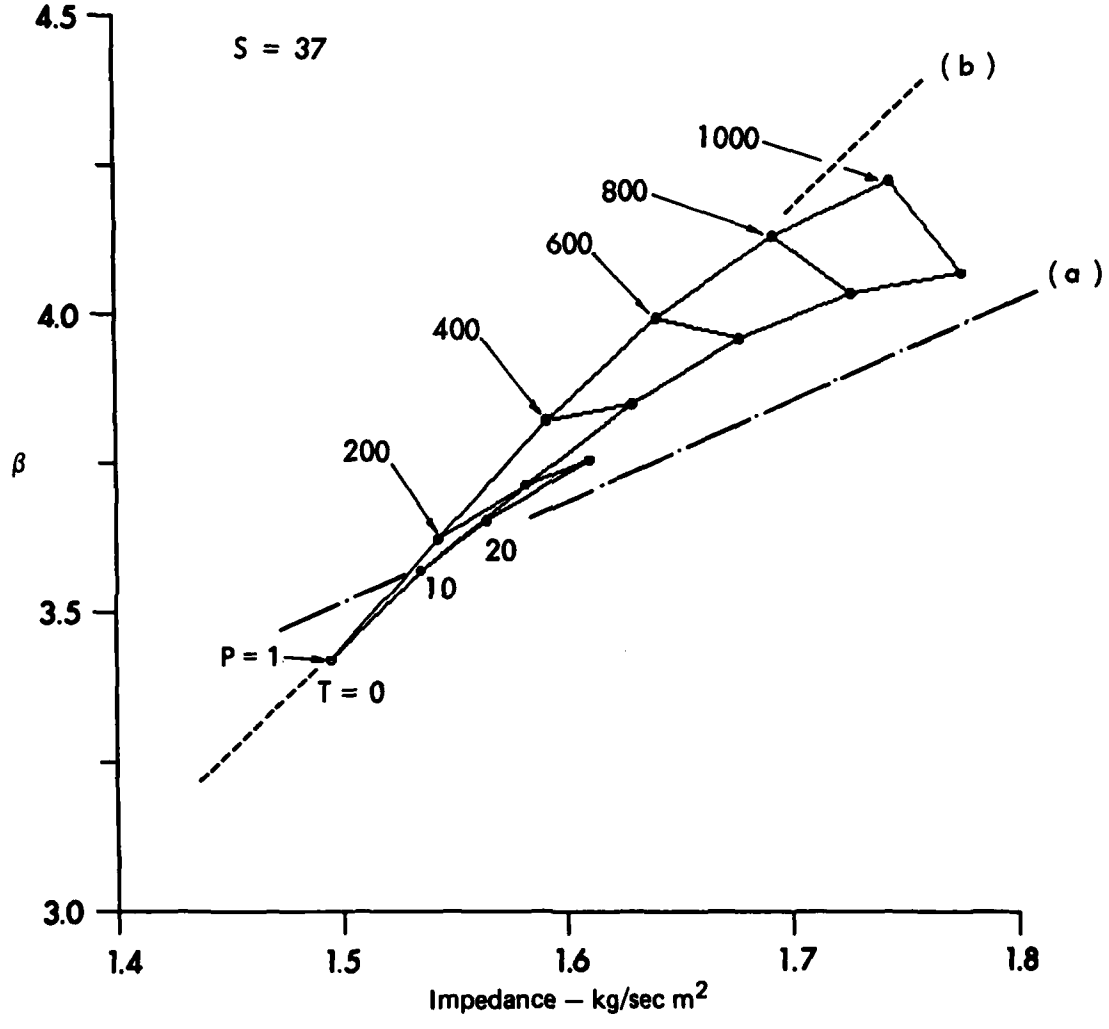

FIGURE C-7
β versus CHARACTERISTIC IMPEDANCE ρc, FOR SEAWATER WITH SALINITY S = 37‰

ARL:UT
AS-84-503
DTB - GA
6 - 11 - 84

APPENDIX D

ASYMPTOTIC RAY RELATIONS FOR SMALL TURNING ANGLES

Relations are derived below for the horizontal range x, the ray path length s, the ray tube area ratio S/S_o, and the nonlinear distance factor G, in terms of the dimensionless change in sound speed,

$$\sigma = \frac{c}{c_o} - 1 \quad .$$

Here c_o is the sound speed at the source; a basic assumption in the analysis is that σ remains a small quantity. We also assume that the gradient of c(z) departs only slightly from a constant value, as explained below.

Horizontal Range

The integral

$$x = \int_{z_o} \frac{dz}{\tan\theta} \qquad \text{(D-1)}$$

may be converted into an integral over c (or σ) by introducing a relation between c and z. A convenient profile description, yielding almost-linear sound speed profiles if the dimensionless parameter b is small, is

$$\frac{z}{a} = \sigma - \frac{1}{2} b\sigma^2 \quad . \qquad \text{(D-2)}$$

This gives the differential relation

$$dz = a(1 - b\sigma)d\sigma \quad , \qquad \text{(D-3)}$$

which is used to substitute for dz in Eq. (D-1).

Constancy of the horizontal phase speed with depth is expressed by

$$\cos\theta = \lambda(1 + \sigma) \quad , \quad (\lambda = \cos\theta_o) \qquad \text{(D-4)}$$

from which it follows that

$$\tan\theta = \frac{1}{\lambda} \frac{[1 - \lambda^2(1 + \sigma)^2]^{1/2}}{(1 + \sigma)} \quad . \qquad \text{(D-5)}$$

We substitute this expression in Eq. (D-1), along with Eq. (D-3), and expand the integrand in powers of the small quantity σ. Retaining only σ and σ^2 terms gives

$$x \simeq a \cot \theta_o \cdot [\sigma + \tfrac{1}{2}(\csc^2\theta_o - b)\sigma^2] \quad ; \tag{D-6}$$

this approximation has a relative accuracy of order σ.

However, the asymptotic result above is not valid for ray angles too close to zero. The next-order (σ^3) term, in the brackets on the right of Eq. (D-6), has a coefficient

$$\tfrac{1}{2}(\cot^4\theta_o + \tfrac{1}{3}\cot^2\theta_o) - \tfrac{1}{3}\, b \quad ; \tag{D-7}$$

it therefore ceases to be small compared with the σ^2 term, whenever θ_o is of order $\sigma^{1/2}$ or smaller.

Ray Path Length

By applying the profile assumption (D-2) to the arc length integral

$$s = \int_{z_o} \frac{dz}{\sin\theta} \quad , \tag{D-8}$$

and making the same approximations as for the horizontal range, we find

$$s \simeq a \csc\theta_o \cdot [\sigma + \tfrac{1}{2}(\cot^2\theta_o - b)\sigma^2] \quad . \tag{D-9}$$

Again, this asymptotic result breaks down for ray angles which are too shallow. In particular, it does not hold through a vertex, since Eq. (D-9) implies only one value of s exists at each depth.

More precisely, Eqs. (D-6) and (D-9) imply that x and s are uniquely determined by the local sound speed; they therefore become invalid when dc/ds changes sign along the ray path.

Ray Tube Area Ratio

Equation (9) gives

$$\frac{S}{S_o} = \frac{x\xi}{x_o^2} \sin\theta \cos\theta_o \quad , \quad \left[\xi = \left(\frac{\partial x}{\partial \theta_o} \right)_z \right] . \tag{D-10}$$

The launch angle derivative (ξ) of the horizontal range follows from differentiating Eq. (D-6). Also, to first-order accuracy in σ,

$$\sin\theta \simeq \sin\theta_o \ (1 - \cot^2\theta_o \cdot \sigma) . \tag{D-11}$$

Combining these results yields the asymptotic approximation

$$\frac{S}{S_o} \simeq \frac{a^2}{x_o^2} \cot^2\theta_o \cdot \sigma^2 \ [1 + (\csc^2\theta_o - b)\sigma] . \tag{D-12}$$

Comparison of Asymptotic and Exact Results

Before proceeding to find an expression for G, it is instructive to check the above asymptotic results against known exact solutions. Analytic solutions are available for certain profiles in the family

$$c = c_o\left(1 + \frac{z}{ma}\right)^m \quad , \quad (m = \text{const.})^\dagger . \tag{D-13}$$

(a) Case m = 1 (linear profile):

$$x = a \sec\theta_o \ (\sin\theta_o - \sin\theta) ; \tag{D-14a}$$

$$s = a \sec\theta_o \ (\theta_o - \theta) ; \tag{D-14b}$$

† The integrals required for m = 1/2,1/3 are given in Gradshteyn and Ryzhik's Table of Integrals,[12] 2·272(3) and (7).

$$\frac{S}{S_o} = \left(\frac{x}{x_o}\right)^2 = \left(\frac{a}{x_o}\right)^2 \sec^2\theta_o \ (\sin\theta_o - \sin\theta)^2 \ . \qquad \text{(D-14c)}$$

(b) Case m = ½ (parabolic profile):

$$x = a \sec^2\theta_o \cdot [(\sin\theta_o \cos\theta_o - \sin\theta \cos\theta) + (\theta_o - \theta)] \ . \qquad \text{(D-15)}$$

(c) Case m = 1/3 (cubic profile):

$$x = a \sec^3\theta_o \cdot [3(\sin\theta_o - \sin\theta) - (\sin^3\theta_o - \sin^3\theta)] . \qquad \text{(D-16)}$$

In order to check the previous asymptotic expansions--obtained using Eq. (D-2) for the sound speed profile--against the exact results given here, we need to relate the profile parameters b and m. Equation (D-13) implies that

$$1 + \frac{z}{ma} = (1 + \sigma)^{1/m} \ , \qquad \text{(D-17)}$$

which may be expanded in powers of σ to yield

$$\frac{z}{a} = \sigma - \frac{1}{2}\left(1 - \frac{1}{m}\right)\sigma^2 + O(\sigma^3) \ . \qquad \text{(D-18)}$$

It follows that to first-order relative accuracy in σ, the profiles in Eqs. (D-2) and (D-13) are equivalent if we set

$$b = 1 - \frac{1}{m} \ . \qquad \text{(D-19)}$$

Expansion of the exact results given for cases (a), (b) and (c) above--a rather lengthy process--demonstrates agreement to first-order accuracy, as expected, with the asymptotic expressions (D-6), (D-9) and (D-12).

Reduced Distance

The reduced distance is defined by

$$\bar{x} = \int_{s_o}^{s} \frac{\alpha}{\alpha_o} \left(\frac{S}{S_o}\right)^{-½} ds' \ . \qquad \text{(D-20)}$$

To convert the integration variable from s to σ, we note that

$$ds = \frac{dz}{\sin\theta} \quad ; \tag{D-21}$$

then using Eqs. (D-3) and (D-11) gives

$$ds \simeq a \csc\theta_o \cdot (1 - b\sigma)(1 + \cot^2\theta_o \cdot \sigma)d\sigma$$

$$\simeq a \csc\theta_o \cdot [1 + (\cot^2\theta_o - b)\sigma]d\sigma \, . \tag{D-22}$$ †

We model the $\alpha(z)$ dependence by the relation

$$\alpha c^n = \text{const.} \; ; \tag{D-23}$$

thus

$$\frac{\alpha}{\alpha_o} = (1 + \sigma)^{-n}$$

$$\simeq 1 - n\sigma, \tag{D-24}$$

to first order in σ.

Relations (D-22), (D-24), and (D-12) are now substituted in the reduced distance integral (D-20) to obtain the $O(\sigma)$ asymptotic result (for $s_o \to 0$)

$$\bar{x} \simeq a \, \sigma_o \csc\theta_o \, (\ln\frac{\sigma}{\sigma_o} - C\sigma) \quad , \quad (\sigma_o \to 0) \quad , \tag{D-25}$$

where

$$C = (n + 1) - \frac{1}{2}(\csc^2\theta_o - b) \, . \tag{D-26}$$

A more instructive version of Eq. (D-25) is obtained by noting that in the limit $\sigma_o \to 0$, the coefficient $a\sigma_o \csc\theta_o$ reduces to s_o, while to first order in σ

† Eq. (D-9) is obtained by integrating this result.

$$-C\sigma \simeq \ln(1 - C\sigma) \ . \qquad \text{(D-27)}$$

Thus the reduced distance is given in terms of σ by

$$\bar{x} \simeq s_o \ln\left[\frac{\sigma}{\sigma_o}(1 - C\sigma)\right] . \qquad \text{(D-28)}$$

This result may be compared with Eq. (9) earlier, which defines the distance modification factor G. The difference is that Eq. (D-28) contains the factor σ/σ_o in the argument of the logarithm, as compared with s/s_o in Eq. (9).

Equation (D-28), with x entirely in terms of σ, would in fact be appropriate if we had chosen to follow Ref. 4 and examine departures of $\bar{x}$ from

$$s_o \ln \frac{\sigma}{\sigma_o} \quad \underline{\text{rather than}} \quad s_o \ln \frac{s}{s_o} \ .$$

(Note that the two expressions coincide only for a linear sound speed profile and small turning angles.) Petukhov and Fridman in their paper[4] used the first expression as their reference; we prefer the second because it leads to a much simpler asymptotic result, as shown below.

The Distance Modification Factor G

The factor G is defined in the present report by

$$\bar{x} = s_o \ln\left(\frac{s}{s_o} G\right) \ ; \qquad \text{(D-29)}$$

its asymptotic value in the case discussed above may be found in terms of σ, by equating arguments in (D-28) and (D-29) and using the arc length expression (D-9). The result is simply

$$G \simeq 1 - (n + \tfrac{1}{2})\sigma \ . \qquad \text{(D-30)}$$

The following points may be noted in relation to Eq. (D-30).

(a) There is no influence of launch angle (θ_o) on the factor G as defined above, up to first order in σ.

(b) Likewise there is no influence of profile curvature (as expressed by the parameter b), up to first order.

(c) These features do not apply if we follow Petukhov and Fridman[4] and study departures of $\bar{x}$ from $s_o \ln(\sigma/\sigma_o)$.

APPENDIX E

THE LIMITING CASE OF VERTICAL PROPAGATION

In an earlier report on the topic of nonlinear sound propagation in a depth dependent ocean, Carlton and Blackstock[1] analyzed the case of vertical propagation using a plane wave model. The purpose of this Appendix is to point out that even the vertical propagation of sound, from a point source in a depth dependent ocean, cannot be properly modeled without considering refraction. Thus the one-dimensional analysis of Carlton and Blackstock, although correct for the plane wave model they assumed, should not be applied to radiation from real sources in the ocean, even at large distances.

Area Variation in a Vertical Ray Tube

For purposes of illustration, we assume a profile in which the sound speed increases linearly with depth:

$$c(z) = c_o(1 + z/a) \ . \qquad \text{(E-1)}$$

The horizontal range (x) in this situation is related to the depth (z) and launch angle (θ_o) by

$$x = a\left\{\tan\theta_o \pm [\sec^2\theta_o - (z/a + 1)^2]^{1/2}\right\} \ . \qquad \text{(E-2)}$$

Figure E1 shows a near-vertical ray (θ_o close to 90°), for which the minus sign in Eq. (E-2) is appropriate (the plus sign applies when the ray has passed through a vertex and is traveling upwards). Since $\cos\theta_o$ approaches zero, it is appropriate to write Eq. (E-2) in asymptotic form as

$$x \simeq z\cot\theta_o \cdot (1 + z/2a) + O(\cos^3\theta_o) \ . \qquad \text{(E-3)}$$

Eq. (E-3) is valid for all z values provided z/a is of order one or less.

It follows that a vertical ray tube, formed by rotating the ray in Fig. E-1 about the z axis, has an area ($S=\pi x^2$) which varies with z as follows:

$$\frac{S}{S_o} = \left(\frac{z}{z_o}\right)^2 \left(1 + \frac{z}{2a}\right)^2 \ , \ (z_o/z \to 0) \ . \qquad \text{(E-4)}$$

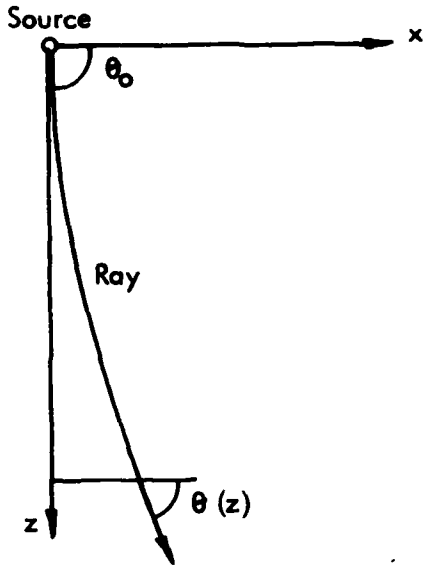

FIGURE E1

DEFINITION SKETCH FOR NEAR-VERTICAL RAYS

Rotation about the z axis forms a ray tube with its axis vertical.

In practical ocean applications, z is small compared with a--in other words the percentage change in sound speed along the ray path is small--and Eq. (E-4) may be approximated by

$$\frac{S}{S_o} \simeq \left(\frac{z}{z_o}\right)^2 \left(\frac{c}{c_o}\right) \qquad \text{(E-5)}$$

in view of Eq. (E-1).

Interpretation of Eq. (E-5)

(a) In a uniform ocean, the c/c_o factor equals unity, and Eq. (E-5) represents spherical spreading.

(b) More generally, wavefronts in a stratified ocean do not spread spherically, even along a vertical propagation path.

(c) In calculating the reduced distance integral

$$\bar{x} = \int_{s_o}^{s} \frac{\alpha}{\alpha_o} \left(\frac{S}{S_o}\right)^{-\frac{1}{2}} ds' \qquad \text{(E-6)}$$

along a vertical ray, it is inconsistent to allow for the vertical variation of α while neglecting the non-spherical spreading factor c/c_o indicated by Eq. (E-5) above.

APPENDIX F

EVALUATION OF THE FACTOR G VIA RAY PATH INTEGRATION

It is convenient to calculate the distance modification factor G directly, rather than by first calculating $\bar{x}$ from Eq. (6) and then inferring G from Eq. (9). In this Appendix we relate G to a ray path integral F, and then discuss the numerical method used to evaluate F.

Equation (6) for the reduced distance may be written as

$$\bar{x} = \int_{s_o}^{s} W(s')\, ds' \quad , \tag{F-1}$$

where the arc length weighting factor W is given by

$$W(s) = \frac{\alpha}{\alpha_o} \cdot \left(\frac{S}{S_o}\right)^{-1/2}$$

$$= s_o A(s) \quad , \quad \text{say.} \tag{F-2}$$

Note that A(s) has dimensions of inverse length. It is independent of the initial distance s_o along the ray, in the limit $s_o \to 0$. By substituting for S/S_o from Eq. (11), we obtain

$$A(s) = \frac{\alpha}{\alpha_o} \left(\frac{\cos\theta}{\cos\theta_o}\right)^{-1/2} (x\xi)^{-1/2} \quad . \tag{F-3}$$

The definition of G, Eq. (9), is

$$\bar{x} = s_o \ln\left(G \cdot \frac{s}{s_o}\right) \tag{F-4}$$

which may be differentiated with respect to s to give

$$\frac{d\bar{x}}{ds} = \frac{s_o}{G} \frac{dG}{ds} + \frac{s_o}{s} \quad . \tag{F-5}$$

Equating the right-hand side to $s_o A(s)$--from Eq. (F-2)--yields

$$\frac{1}{G} \frac{dG}{ds} = A(s) - \frac{1}{s} \quad . \tag{F-6}$$

It follows that

$$G = \exp F(s), \tag{F-7}$$

where

$$F(s) = \int_0^s f(s')ds' \quad ; \quad f(s) = A(s) - \frac{1}{s} \ . \tag{F-8}$$

The advantage of this formulation, in computational terms, is that the integrand in Eq. (F-8) is well-behaved as s' tends to zero, unlike W(s') in the reduced distance integral (F-1) which is singular. Moreover, the starting distance s_o does not appear in Eqs. (F-7) and (F-8).

A useful check on the numerical values of F obtained for small distances (or small turning angles) follows from the asymptotic expansion

$$f(s) = A(s) - \frac{1}{s} \simeq \frac{-(n + \frac{1}{2})}{a} \sin \theta_o \ , \quad (s \to s_o) \tag{F-9}$$

which is based on a locally linear profile approximation, as in Eq. (24), with αc^n constant. The derivation is straightforward using Eqs. (D-9) and (D-12). Equation (F-9) makes it clear that f(s) tends to a constant value as s tends to zero.

The numerical integration scheme used to evaluate Eq. (F-8) is described next. Since the quantities needed to evaluate f(s) are available at each step of the MEDUSA ray tracing program,[11] it is convenient to use the ray-tracing steps (which are of uneven length) as numerical integration steps in evaluating Eq. (F-8). We use the second-order approximation

$$\int_{s_{i-1}}^{s_i} f(s)ds \simeq \frac{1}{2} h(f_i + f_{i-1}) - \frac{1}{12} h^2(f_i' - f_{i-1}') \ , \tag{F-10}$$

where h is the step size $(s_i - s_{i-1})$ in arc length. For the first integration step, we use

$$\int_0^{s_1} f(s)ds \simeq s_1 f(s_1) \qquad \text{(F-11)}$$

since f(s) is asymptotically constant as s tends to zero.

The values of the derivative f' (s) required by Eq. (F-10) are calculated as follows. Logarithmic differentiation of Eq. (F-2) along the ray path yields

$$f'(s) = A(s)B(s) + \frac{1}{s^2} \ , \qquad \text{(F-12)}$$

where

$$B(s) = \frac{\alpha'(z)}{\alpha(z)} \sin\theta + \frac{1}{2} z_x z_{xx} \cos^3\theta - \frac{1}{2}\left(\frac{1}{x} + \frac{\zeta_x}{\zeta}\right)\cos\theta \ . \qquad \text{(F-13)}$$

In the above equation, x subscripts denote derivatives with respect to horizontal range (x), following the ray path. In particular,

$$z_x = \tan\theta \ . \qquad \text{(F-14)}$$

The quantities needed to evaluate A(s) and B(s) are provided by the ray tracing program MEDUSA at each step. Thus the ray tracing program is run first, and the appropriate output stored for transfer to the integration program, which then evaluates $F(s_i)$ at each step. Values of $G(s_i)$ finally follow from

$$G(s_i) = \exp F(s_i) \ . \qquad \text{(F-15)}$$

ACKNOWLEDGMENTS

The author is grateful for the advice and encouragement of Dr. David T. Blackstock, ARL:UT, on whose initiative his stay at ARL:UT during January-July 1983 was arranged.

REFERENCES

1. T. W. Carlton and D. T. Blackstock, "Propagation of Plane Waves of Finite Amplitude in Inhomogeneous Media with Applications to Vertical Propagation in the Ocean," Applied Research Laboratories Technical Report No. 74-31 (ARL-TR-74-31), Applied Research Laboratories, The University of Texas at Austin (1974).

2. E. N. Pelinovskii, Yu. V. Petukhov, and V. E. Fridman, "Approximate Equations for the Propagation of Strong Acoustic Signals in the Ocean," Izv. Acad. Sci. USSR, Atmos. Oceanic Phys. 15, 299-304 (1979).

3. V. E. Fridman, "Propagation of a Strong Sound Wave in a Plane-Layered Medium," Sov. Phys.-Acoust. 22, 349-350 (1976).

4. Yu. V. Petukhov and V. E. Fridman, "Propagation of Blast Waves in a Stratified Ocean," Izv. Acad. Sci. USSR, Atmos. Oceanic Phys. 15, 917-922 (1979).

5. C. C. Leroy, "Formulas for the Calculation of Underwater Pressure in Acoustics," J. Acoust. Soc. Am. 44, 651-653 (1968).

6. C. Eckart, "Properties of Water, Part II. The Equation of State of Water and Sea Water at Low Temperatures and Pressures," Am. J. Sci. 256, 225-240 (1958).

7. W. Wilson and D. Bradley, "Specific Volume of Sea Water as a Function of Temperature, Pressure and Salinity," Deep-Sea Research 15, 355-363 (1968).

8. W. D. Wilson, "Equation for the Speed of Sound in Sea Water," J. Acoust. Soc. Am. 32, 1357 (1960).

9. D. T. Blackstock, "Three Topics in Nonlinear Acoustics," Applied Research Laboratories Technical Report No. 76-17 (ARL-TR-76-17), Applied Research Laboratories, The University of Texas (1976).

10. C. C. Leroy, "Development of Simple Equations for Accurate and More Realistic Calculation of the Speed of Sound in Seawater," J. Acoust. Soc. Am. 46, 216-226 (1969).

11. T. L. Foreman, "Ray Modeling Methods for Range Dependent Ocean Environments," Applied Research Laboratories Technical Report No. 83-41 (ARL-TR-83-41), Applied Research Laboratories, The University of Texas at Austin (1983).

12. I. S. Gradshteyn and I. M. Ryzhik, Table of Integrals, Series and Products (4th edn.) (Academic Press, New York, 1965).

13. D. F. Fenner and P. J. Bucca, "The Sound Velocity Structure of the North Atlantic Ocean," Naval Oceanographic Office Informal Report No. 71-13, unpublished report (1971).

14. U. S. Naval Oceanographic Office, Environmental-Acoustics Atlas of the Caribbean Sea and Gulf of Mexico, Vol. 2 (Washington, D.C., 1972).

23 April 1984

DISTRIBUTION LIST FOR
ARL-TR-84-11
under Contract N00014-82-K-0805

Copy No.

Office of Naval Research
800 North Quincy Street
Arlington, VA 22217
1 Attn: R. M. Fitzgerald, Code 425UA
2 L. E. Hargrove, Code 412

3 - 14 Defense Technical Information Center
Cameron Station, Building 5
5010 Duke Street
Alexandria, VA 22314

Naval Research Laboratory
Department of the Navy
Washington, DC 20375
15 - 20 Attn: Director
21 B. E. McDonald

Naval Ocean Research and Development Activity
NSTL Station, MS 39529
22 Attn: W. A. Kuperman
23 K. Gilbert

Naval Underwater Systems Center
New London Laboratory Detachment
New London, CT 06320
24 Attn: Technical Center
25 R. H. Mellen
26 M. B. Moffett

NASA Langley Research Center
Mail Stop 460A
Hampton, VA 23665
27 Attn: Harold Lester

Naval Ocean Systems Center
San Diego, CA 92152
28 Attn: F. M. Pestorius

Distribution List for ARL-TR-84-11 under Contract N00014-82-K-0805
(Cont'd)

Copy No.

Naval Postgraduate School
Monterey, CA 93940
29 Attn: Technical Library
30 A. B. Coppens
31 S. L. Garrett
32 H. Medwin

Naval Research Laboratory
P. O. Box 8337
Orlando, FL 32856
33 Attn: A. L. Van Buren

Naval Coastal Systems Center
Panama City, FL 32407
34 Attn: D. H. Trivett

Brown University
Department of Physics
Providence, RI 02912
35 Attn: P. J. Westervelt

University of California
Lawrence Livermore Laboratory
Theoretical Physics, L-71
P. O. Box 808
Livermore, CA 94550
36 Attn: S. I. Warshaw

University of California at Los Angeles
Physics Department
Los Angeles, CA 90024
37 Attn: I. Rudnick

Georgetown University
Physics Department
Washington, DC 20057
38 Attn: W. G. Mayer

Georgia Institute of Technology
School of Mechanical Engineering
Atlanta, GA 30332
39 Attn: J. H. Ginsberg
40 A. D. Pierce
41 P. H. Rogers

Distribution List for ARL-TR-84-11 under Contract N00014-82-K-0805
(Cont'd)

Copy No.

Kalamazoo College
Department of Physics
Kalamazoo, MI 49007
42 Attn: W. M. Wright

University of Mississippi
Physics Department
University, MS 38677
43 Attn: H. E. Bass

The Pennsylvania State University
Applied Research Laboratory
University Park, PA 16802
44 Attn: S. McDaniel

University of Tennessee
Department of Physics
Knoxville, TN 37916
45 Attn: M. A. Breazeale

Virginia Polytechnic and State University
Engineering Science and Mechanics
Blacksburg, VA 24061
46 Attn: M. S. Cramer
47 A. Nayfeh

Yale University
Department of Engineering
Mason Laboratory
9 Mill House Avenue
New Haven, CT 06520
48 Attn: R. E. Apfel

University of Miami/RSMAS
4600 Rickenbacker Causeway
Miami, FL 33149
49 Attn: F. D. Tappert

Jet Propulsion Laboratory
4800 Oak Grove
Pasadena, CA 91103
50 Attn: T. G. Wang

Distribution List for ARL-TR-84-11 under Contract N00014-82-K-0805
(Cont'd)

Copy No.

	Raytheon Co. P. O. Box 360 Portsmouth, RI 02871
51	Attn: R. D. Pridham
	Chief Defence Research Establishment Atlantic P. O. Box 1012 Dartmouth, Nova Scotia CANADA
52	Attn: H. M. Merklinger
	University of Toronto Institute for Aerospace Studies 4925 Dufferin St. Downsview, ON M3H 5TC CANADA
53	Attn: W. G. Richarz
54	I. I. Glass
	Technical University of Denmark Industrial Acoustics Laboratory Building 352 DK-2800 Lyngby DENMARK
55	Attn: L. Bjørnø
	University of Bath School of Physics Claverton Down Bath BA2 7AY ENGLAND
56	Attn: H. O. Berktay
	University of Leeds Applied Math. Studies Leeds, Yorkshire LS2 9JT ENGLAND
57	Attn: D. G. Crighton
	Institute of Sound and Vibration Research The University Southampton SO9 5NH ENGLAND
58 - 67	Attn: C. L. Morfey

Distribution List for ARL-TR-84-11 under Contract N00014-82-K-0805
(Cont'd)

Copy No.

Admiralty Underwater Weapons Establishment
Portland
Dorset DT5 2
ENGLAND
68 Attn: D. E. Weston

Nagoya University
Department of Electrical Engineering
Furo-Cho
Chikusa-Ku
Nagoya
JAPAN
69 Attn: T. Kamakura

Osaka University
The Institute of Scientific and Industrial Research
8-1, Mihogaoka, Ibaraki
Osaka 567
JAPAN
70 Attn: A. Nakamura

Instituto de Acustica
Laboratorio de Ultrasonidos
Consejo Superior de Investigaciones Cientificas
Serrano, 144
Madrid-6
SPAIN
71 Attn: J. A. Gallego-Juarez

Universitet I Bergen
Matematisk Institutt
Allegaten 53-55
5000 Bergen
NORWAY
72 Attn: Sigve Tjøtta and
Jacqueline Naze Tjøtta

73 Anthony M. Bedford, ARL:UT

74 Yves H. Berthelot, ARL:UT

75 David T. Blackstock, ARL:UT

76 I. Busch-Vishniac, ARL:UT

77 Frederick D. Cotaras, ARL:UT

Distribution List for ARL-TR-84-11 under Contract N00014-82-K-0805 (Cont'd)

Copy No.	
78	C. Robert Culbertson, ARL:UT
79	Glen E. Ellis, ARL:UT
80	James M. Estes, ARL:UT
81	Terry L. Foreman, ARL:UT
82	Mark F. Hamilton, ARL:UT
83	James A. Hawkins, Jr., ARL:UT
84	John M. Huckabay, ARL:UT
85	David P. Knobles, ARL:UT
86	T. G. Muir, ARL:UT
87	David A. Nelson, ARL:UT
88	M. Cecile Penland, ARL:UT
89	James A. TenCate, ARL:UT
90	Arnold J. Tucker, ARL:UT
91	Library, ARL:UT
92 - 101	Reserve, ARL:UT

END

FILMED